Response to RAI Background Section

<u>Executive Summary</u>

The NRC has requested additional information regarding DOE's methodologies and estimates of drift degradation and accumulated rubble volume for emplacement drifts subjected to thermal stresses and time-dependent strength changes (Volume 3 – Postclosure Chapter 2.2.1.2.1 Scenario Analysis, 1st Set (RAIs 1 through 6), Exclusion of FEP 2.1.07.02.0A). Detailed responses to each of the six RAIs are given in Enclosures 2 through 7.

However, prior to stating its request for additional information, the NRC provided an additional section entitled <u>Background</u> in which several technical viewpoints were expressed regarding the model that DOE has used to evaluate drift degradation. In the following, DOE has reproduced the <u>Background</u> statements, paragraph by paragraph, with an accompanying response to each. It is intended that this discussion will assist the NRC in better understanding the logic supporting DOE's technical basis.

<u>NRC Background Statement, Paragraph 1:</u>

The Features, Events, and Processes (FEP) 2.1.07.02.0A Drift Collapse is excluded from the performance assessment model based on low consequence (Safety Analysis Report Section 2.2, Table 2.2-5). The technical basis used to support this screening decision (Sandia National Laboratories, 2008a) relies, in part, on a numerical model that evaluates the mechanical effects on drift walls in response to heating from waste emplacement or time-dependent weakening of the surrounding rock (Bechtel SAIC Company, 2004). The NRC staff considers that the technical bases of the screening argument are not sufficient to support exclusion of the FEP from the performance assessment model.

<u>DOE Response:</u>

DOE firmly supports the sufficiency of the basis used in excluding FEP 2.1.07.02.0A, Drift Collapse, from the performance assessment (BSC 2004, Table 6-51). The technical bases for this screening are sufficient because DOE's predictions of stable tunnels during the early years after emplacement, in which the peak temperatures and thermally induced stresses are reached, are consistent with tunnel stability in high-stress environments, and consistent with extensive experience in the mining and civil underground construction industries. Collectively, the responses to RAIs 3.2.2.1.2.1-001 through 3.2.2.1.2.1-006 (Enclosures 2 through 7) provide additional confidence that the Yucca Mountain Project has not underestimated the quantity of rubble due to nominal drift degradation processes, and provide a strong basis for the exclusion of FEP 2.1.07.02.0A from total system performance assessment.

NRC Background Statement, Paragraph 2:

The DOE model used to evaluate drift degradation due to thermal loading or time-dependent rock weakening has several inherent assumptions and limitations that may underestimate the extent of degradation and the quantity of accumulated rubble in a drift. The model represents the rock mass surrounding a drift as an assemblage of randomly oriented polygonal elastic blocks that may slip or separate only at block interfaces (Safety Analysis Report, Section 2.3.4.4.5.3; Bechtel SAIC Company, 2004, Sections 6.4.2.1 and 7.6.4). The block interfaces in the model are generated randomly and, therefore, are generally oblique to potential failure surfaces for rock spalling. Also, the blocks are generally large enough to traverse potential spalling zones. The combined effects of the assumptions of randomly oriented block contacts, elastic behavior (therefore, infinite strength) of blocks, and large block sizes appear to prevent the development of fractures that could propagate across blocks and cause spalling. Therefore, the model may indicate a stable drift opening even if the boundary of the opening is subjected to stresses high enough to potentially cause spalling. For example, a DOE report on thermal-mechanical analysis (Sandia National Laboratories, 2008b, Section 6.4.1.5) shows drift walls and roofs subjected to stresses greater than the unconfined compressive strength of the surrounding rock. However, DOE concluded that the drifts are stable because the model does not predict rockfall explicitly.

DOE Response:

The line of reasoning expressed above leads to a conclusion that, when stresses around underground excavations planned for the Yucca Mountain Repository exceed the unconfined compressive strength (UCS) of the host rock mass, then (1) such excavations will be unstable, and (2) spalling will be the dominant failure mechanism.

This line of reasoning is flawed because it leads to over-prediction of rockfall. First, spalling is not the failure mode in fractured rock masses such as the lithophysal units that host most of the repository, as discussed in Section 2.2. Second, the body of empirical evidence taken from extensive mining and construction experience demonstrates that excavations with stresses at the tunnel periphery that exceed the rock UCS are stable (Section 1). Third, even where spalling is the dominant failure mode in massive rock because the rock mass is stressed above the UCS, such drifts stabilize under a wide range of conditions and do not demonstrate progressive failure, as shown by empirical evidence in Section 2.1. Technical approaches for making predictions of drift stability, consistent with mining and civil industries, are summarized below, and these are the bases used for DOE's predictions.

NRC refers to "inherent assumptions" when describing block size and fracture orientation, but these are more accurately characterized as modeling inputs that were carefully selected to represent conditions observed in situ at Yucca Mountain.

NRC Background Statement, Paragraph 4:

The model relies on a novel technique for performing coupled analysis of rock deformation, fracturing, and failure. In contrast to commonly used models for rock deformation, the DOE model does not directly use the characterized rock-mass fracture geometry and mechanical properties. Instead, the values of the model parameters were determined by calibrating the elastic behavior of the model against the elastic behavior of the rock mass based on laboratory unconfined compression testing. The inelastic behavior of the model (e.g., relationship between dilatational and shearing strains), however, was not calibrated. The inelastic behavior appears to be important in modeling the interactions among fractured and unfractured rock and pieces of broken rock, therefore, it appears to affect the calculation of rock failure and potential rubble formation.

DOE Response:

In the paragraph above, NRC mischaracterizes three aspects of DOE's drift stability models: (1) The numerical approach used by DOE to represent the lithophysal rock mass does not involve "a novel technique," but does rely upon numerical "experiments" to calibrate against material properties measured in the laboratory to supplement rock mass property development. The basic modeling approach has been in use for approximately 25 years as explained below in Section 3. (2) In contrast to assertions above, the DOE model uses underground observations extensively to characterize rock-mass fracture geometry, quantify lithophysal porosity, and assign mechanical properties as discussed in *Drift Degradation Analysis* (BSC 2004, Sections 6.1 and 7.6.4, and Table E-11). (3) While NRC asserts insufficient calibration, the model was, in fact, calibrated to both elastic and inelastic behavior of the rock mass based on laboratory testing as described in the response to RAI 3.2.2.1.2.1-005 (Enclosure 6).

NRC Background Statement, Paragraph 5:

To support the use of the model, empirical observations were presented of roof spalling from the unsupported portion of the drift-scale heater test (Safety Analysis Report, Section 2.3.4.4.5.3.2). However, the nature and extent of the spalled rock from the heater test have not been characterized or quantified. Also, the simulation of the drift scale heater test for model support (Bechtel SAIC Company, 2004, Section 7.6.5.3) did not account for the effects of ground support installed in the test tunnel, the three dimensional nature of the tunnel, or an extrapolation of the test results to time scales representative of the thermal period in the repository.

DOE Response:

Predictions with the DOE models are consistent with the observed rockfall volume at the completion of the Drift Scale Test. Supplemental verification calculations have confirmed empirical observations and modeling experience that the ground support does not alter the original validation of the DOE models. Three-dimensional effects are also not expected to be significant, as explained in the response to RAI 3.2.2.1.2.1-006 (Enclosure 7).

1.0 Introduction

A general introduction is provided here to demonstrate that the DOE predictions of drift stability during the thermal period and beyond are consistent with extensive experience gained in the mining and civil underground construction industries. The DOE model used to evaluate drift degradation in lithophysal units due to thermal loading or time-dependent rock weakening does not underestimate the extent of degradation and the quantity of accumulated rubble in a drift. The modeling inputs that (1) the Voronoi block model can fail only along randomly oriented surfaces, (2) the individual blocks are elastic, and (3) the average block size is 300 mm, do not prevent the development of fractures and are justified and consistent with the actual behavior of the lithophysal rock mass, as explained in the response to RAI 3.2.2.1.2.1-001 (Enclosure 2). The process used to calibrate the time-dependent strength degradation and nonlinear material parameters for the UDEC model to laboratory test data is explained in the responses to RAIs 3.2.2.1.2.1-002 (Enclosure 3) and 3.2.2.1.2.1-005 (Enclosure 6). Spalling is not a relevant failure mechanism in the lithophysal rock mass, which is not a massive rock (Hoek et. al. 2000, Section 10.1), as explained in Section 2.

Observation of elastic stresses that are greater than the unconfined compressive strength at the drift walls does not necessarily result in an unstable or collapsed excavation (Jaeger and Cook 1979, Section 18.2). The strength of the rock under confined conditions is greater than the unconfined compressive strength. That is why some plots in a DOE report on thermal-mechanical analysis (SNL 2008, Section 6.4.1.5) show drift walls and roofs subjected to stress greater than the unconfined compressive strength of the surrounding rock. Those stresses occur either away from the wall or roof surfaces or around sharp corners, where confined stress conditions exist.

Section 2 provides an overview of the failure mechanisms for tunnels and mine excavations in massive and brittle hard rock masses and in fractured rock masses. UDEC predictions of stable excavations after yielding of rock at the wall of an excavation are consistent with numerous rock mechanics textbooks, standard rock mechanics reference works, and underground mining experience. The response to RAI 3.2.2.1.2.1-003 (Enclosure 4) provides additional details on the inelastic behavior of the host rock surrounding a tunnel or excavation. Section 3 summarizes the numerical models used to analyze drift degradation.

2.0 Mechanism for Failure and Rockfall in Tunnels and Mine Excavations

In highly-stressed rock masses, yielding of the rock at the periphery of a tunnel will occur if the tangential stress exceeds the rock mass uniaxial compressive strength. Two basic mechanisms of rock failure are expected for the Yucca Mountain repository rock types: potential brittle spalling response in the massive nonlithophysal rock units, and more ductile yielding in the lithophysal rock units. The effect of rock yielding on tunnel stability and potential breakout and rockfall will depend on the ratio of the stress to strength as well as the brittleness (or ductility) of the rock.

If the rock is brittle and massive, such as the nonlithophysal rock mass, rock yielding could result in spalling, and breakout of the tunnel surface. However, even in this case, practical experience indicates that a stable tunnel configuration is achieved for a wide range of conditions after the breakout reaches a finite depth. A discussion on practical mining observations of the spalling/slabbing behavior of tunnels and large span mining excavations in hard, brittle, and massive rocks in which the induced stresses exceed the rock mass strength is given below. Spalling breakouts in brittle rocks (even when tunnels are unsupported) do not exceed approximately one tunnel radius, as explained in Section 2.1.

If the rock is sufficiently ductile (typically due to the presence of closely-spaced fractures), yielding will result in some strength loss of the rock near the boundary, accompanied by redistribution of stress concentrations away from the boundary to where confinement and rock strength are greater and stable conditions are maintained. In those cases, yielding of rock will result in deformation of the tunnel, but may not result in any instability or rockfall. Jaeger and Cook (1979, Section 18.2), in the classic textbook on rock mechanics, *Fundamentals of Rock Mechanics*, state: "However, in many excavations, especially those resulting from mining, it is not possible to keep stresses everywhere in the rock less than its strength. Neither does experience indicate that this is necessary to ensure stability of the excavations." As described in detail in response to RAI 3.2.2.1.2.1-001 (Enclosure 2), the lithophysal rock mass behaves in a more ductile fashion due to the presence of an extensively fractured rock matrix as well as the lithophysal voids themselves. Therefore, the lithophysal rock is not massive, and thus will not be subject to a spalling failure mechanism, but rather a general yielding response as described above.

2.1 Empirical Evidence for Prediction of Depth of Failure and Breakout of Excavations in Massive and Brittle Hard Rock Masses

The nonlithophysal rock mass at Yucca Mountain makes up approximately 15% of the repository host rock mass. The nonlithophysal rock is strong, hard, and brittle, and the pre-existing cooling fractures are generally non-persistent with short trace lengths (BSC 2004, Section 6.1.4.1). According to the leading authorities in the field of rock mechanics, Hoek et al. (2000, Section 10.1): "In all cases [where spalling is observed] the rock surrounding the excavation is brittle and massive. In this context massive means that there are very few discontinuities such as joints or, alternatively, the spacing between the discontinuities is of the same order of magnitude as the dimensions of the opening." Therefore, brittle fracture and spalling is a potential failure mechanism in the nonlithophysal rocks when subjected to stresses in excess of their compressive strength. In brittle, massive rock masses, failure by local spalling or slabbing will initiate at the tunnel surface and, typically, take the form of fractures oriented parallel to the tunnel surface. This failure will continue to some depth, d_f (see inset, Figure 1), until a new equilibrium state is reached. Typically, the failure region will take the form of a v-shaped or elliptical notch whose depth at equilibrium, d_f, depends on the ratio of the maximum tangential stress (σ_{max}) to the laboratory uniaxial compressive strength (σ_c).

Martin et al. (1999, Section "Depth of stress-induced failure") performed a review of observed depths of failure from "overstressed" tunnels in mines worldwide, and determined that d_f is linearly related to the ratio (σ_{max}/σ_c) as shown in Figure 1. The rock masses comprising the case histories shown in Figure 1 ranged from sedimentary siltstones (σ_c ~ 40 MPa) to igneous granites (σ_c ~ 240 MPa). Thus, this figure pertains to a wide range of massive rock types and strengths. As seen in this figure, this database includes case examples in which the value of σ_{max} is greater than the laboratory uniaxial compressive strength of the rock and indicates a depth of failure of slightly less than one tunnel radius before self-stabilization of the tunnel geometry.

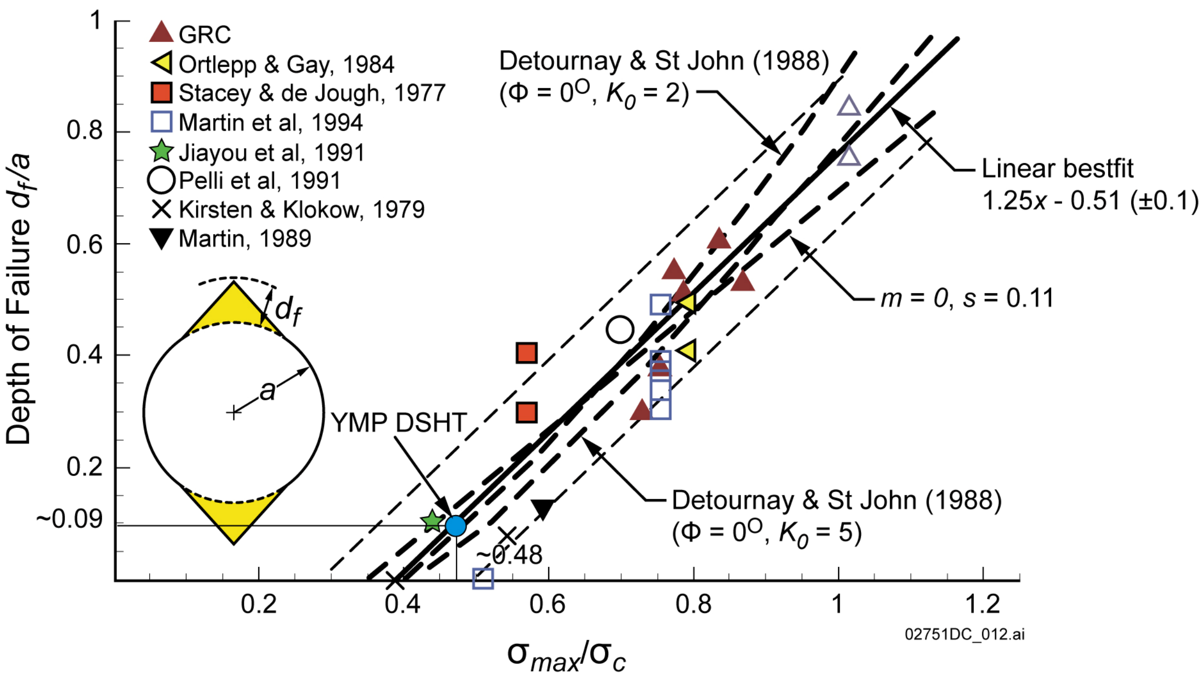

Source: Kaiser et al. 2000, Figure 3.12.

Figure 1. Relationship of the Depth of Failure as a Function of the Maximum Boundary Stress to Uniaxial Compressive Strength Ratio for Tunnels in Hard Rock

This practical evidence of drift breakout is directly applicable to emplacement drift stability under combined in situ and thermally induced stress. The reason is that there is essentially no mechanical difference between the stress concentrations at the tunnel resulting from an in situ stress state applied at "infinite" boundaries or the combined thermal and in situ stresses occurring at any particular point in time in the repository environment. Even the effect of change in drift profile on rock temperatures and thermally induced stresses would have a second order effect on depth of breakout as predicted by empirical data shown in Figure 1. It certainly would not result in progressive breakouts. Because of the relatively small temperature gradient, the increase in temperature at the tip of the breakout due to a 1-m breakout would be approximately 10°C (BSC 2004, Figure 6-140), which would result in a stress increase of only approximately 5%. Thus, the empirical curve shown in Figure 1 is also applicable to thermally induced breakouts.

A question relevant to emplacement drift stability in nonlithophysal rock at Yucca Mountain is, "Why do these tunnels reach a self-stabilizing equilibrium state with depth of failure of less than one tunnel radius when maximum applied compressive stresses are greater than the compressive strength of the rock mass?" In other words, why do even tunnels in brittle, massive rocks in practice equilibrate and not demonstrate progressive failure and collapse to great depths as the rock mass in the periphery fails? One thing that is known is that the finite depth of failure is not achieved due to the presence of ground support (e.g., rockbolts, wire mesh, etc.); it is well known that ground support has little impact on the depth of failure. As stated by Kaiser et al. (2000, Section 3.2.2), "It is of practical importance to realize that in hard rock σ_{max} and therefore the depth of failure is insensitive to the support pressure applied at the excavation wall (for an extreme support pressure of 2 MPa the depth of failure is only reduced by 2 to 3%)."

Perhaps the most highly documented investigation of drift spalling and associated depth of failure is from the Underground Research Laboratory (URL), which was excavated as part of the Canadian nuclear waste program (see, for example, Hoek et al. 2000, Section 10.3.4). Here, a 3.5-m diameter circular tunnel was excavated in highly stressed, unfractured, and brittle granite by perimeter line drilling and mechanical breakage to avoid any blast-damage effects. Failures in the tunnel roof and floor were observed immediately after advancing the face and progressed as the tunnel advanced, forming notch-shaped breakouts. The breakouts were excavated to solid rock to reveal their extent and shape (Figure 2). The breakouts (shown as blue squares and denoted as "Martin et al, 1994" in Figure 1) equilibrated without ground support after several months at a maximum depth of about 30% to 40% of the tunnel radius (Martin et al. 1999, Table 1), consistent with a ratio of maximum boundary stress to the rock mass uniaxial compressive strength of about 0.75, and consistent with other data presented in Figure 1. No further increase in the notch size has been observed since this time (1992), although the drift has remained unsupported.

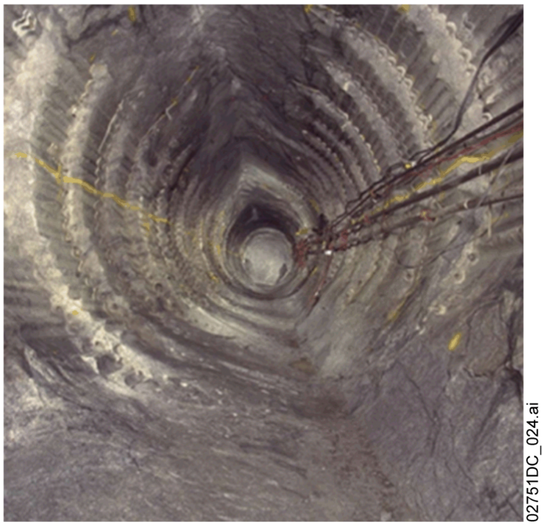

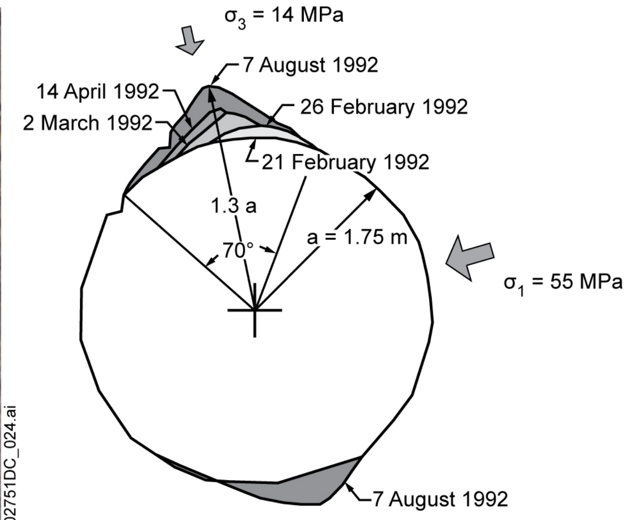

Source: Left figure: Martin 1997, Figure 35a; right figure: Hoek et al. 2000, Figure 10.8.

NOTE: Tunnel overbreak, which was removed by mechanical means, is shown in the geometry at self-sustained equilibrium.

Figure 2. Observed Spalling Overbreak Developed in a 3.5-m Diameter Mechanically Excavated Tunnel in Massive Granite at the Underground Research Laboratory in Canada

In addition to tunnels, examples of large mined openings at great depth in hard rock that are unsupported and equilibrate without progressive collapse are commonplace. Sublevel open stoping is a common mining method employed in many mining districts to extract deep (in excess of 1,500 m) ore reserves. This method involves opening of unsupported, flat-roof rectangular spans typically 25 m across, by mass blasting large cavities. These openings will often exhibit a degree of overbreak, but attain a stable, arched roof span. Standard, empirically based design methodologies (e.g., Mawdesley 2002, Section 2.7) have been developed for prediction of the stable span dimensions for these large openings based on the rock mass stress to strength ratios, the geometry of natural jointing and excavation orientation and span.

2.2 Mechanism of Tunnel Failure in Fractured Rock Masses

The lithophysal rock mass (primarily the Tptpll unit) at Yucca Mountain makes up roughly 85% of the repository emplacement area. As described in the response to RAI 3.2.2.1.2.1-001 (Enclosure 2), the lithophysal rock consists of the same rock matrix as the nonlithophysal material, but it is ubiquitously fractured with closely spaced, non-persistent cooling joints. In addition, the matrix contains from 10% to 30% porosity made up of small lithophysal cavities. Laboratory compression testing of large rock cores containing many lithophysae show that the samples fail in an elastic-plastic and more ductile mode by extension of pre-existing fractures to interconnect and deform the lithophysal voids. Tunnels in fractured rock masses equilibrate when subjected to high stresses due to a process of localized rock mass yield and stress redistribution (e.g., Carranza-Torres and Fairhurst 1999). When the rock mass in the periphery of the tunnel yields, it is accompanied by a loss of cohesion as the solid rock bridges between discontinuous fractures break. This strength loss is greatest at the tunnel periphery, and decreases with distance into the rock mass until it becomes zero in the essentially "infinite" elastic region surrounding the tunnel. This local yielding causes a shift in induced stresses away from the tunnel surface to more confined and elastic regions within the rock mass where they can be sustained without further failure. This allows excavation stability to be restored, since some level of cohesion can be retained (due to finite brittleness) and high induced stresses are able to exist under more confined conditions (without causing further yield). Depending on rock brittleness (i.e., the rate of post-peak strength reduction as a function of strain), some of the yielded material can become unstable and result in rockfall. Martin et al. (1999, Section "Application of Hoek-Brown brittle parameters," Subsection "Elastic versus plastic analyses") have demonstrated that elastic-plastic material models of the rock mass that employ a mechanism of plastic failure characterized by a loss of cohesion and finite post-peak-strength brittleness are able to represent this process of failure near the opening and stress redistribution.

3.0 Methods DOE Used to Analyze Drift Stability

The numerical models used by DOE to represent this process of yielding and stress redistribution under combined thermal and in situ stress loading are described in *Drift Degradation Analysis* (BSC 2004, Sections 6.4 and 7.6) and in the response to RAI 3.2.2.1.2.1-001 (Enclosure 2). These models include standard tunnel stability assessment programs FLAC (continuum) and UDEC (discontinuum). These two approaches provide the same overall representation of the lithophysal rock mass as an elastic-plastic, cohesion softening material for modeling of rock mass failure mechanisms. Both approaches were used to conduct sensitivity studies of drift stability over a wide range of potential lithophysal porosities and associated rock mass strength and stiffness conditions. The FLAC continuum approach to modeling of tunnel stability is more widely used, but the UDEC discontinuum approach affords the ability to examine not only the general depth of failure, but also how the rock mass may fracture and form rockfall under thermal, seismic, and gravitational loading.

The UDEC discontinuum representation has been in use for about 25 years, and typically uses numerical "experiments" to calibrate the discontinuum response to material properties measured in the laboratory. The UDEC modeling approach employed here was originally developed by Plesha and Aifantis (1983) to simulate the shear and tensile fracturing of rock under applied loading . The approach was then extended to simulate the failure response and associated stress-strain behavior of concrete beams (Lorig and Cundall 1987). In this work, a UDEC Voronoi polygonal model of reinforced concrete was successfully validated against the stress-strain and fracturing response of laboratory tests of concrete samples in unconfined compression testing and static and dynamic testing of beams. Additionally, the UDEC predictions of rockfall volume are consistent with the observed rockfall volume from the Drift Scale Test, as shown in the response to RAI 3.2.2.1.2.1-006 (Enclosure 7). Further details of the calibration process are in the response to RAI 3.2.2.1.2.1-005 (Enclosure 6). The DOE approach has been published in the form of two detailed technical papers in a refereed international rock mechanics journal (Lin et al. 2007; Damjanac et al. 2007).

4.0 Concluding Remarks

The DOE has used multiple approaches to analyze the stability of drifts in lithophysal units in response to thermal loading and time-dependent strength degradation. These approaches include (1) the UDEC model, in which the rock mass is represented as an assembly of polygonal blocks, (2) a continuum elastic model with FLAC, and (3) an elastic-plastic model with FLAC. The results from these models are consistent with experience from the mining industry for the stability of underground excavations.

Collectively, the responses to RAIs 3.2.2.1.2.1-001 through 3.2.2.1.2.1-006 (Enclosures 2 through 7) provide confidence that the Yucca Mountain Project has not underestimated the quantity of rubble due to nominal drift degradation processes, providing a strong basis for the exclusion of FEP 2.1.07.02.0A from total system performance assessment.

5.0 References

BSC (Bechtel SAIC Company) 2004. *Drift Degradation Analysis*. ANL-EBS-MD-00027 REV 03 ACN 03 ERD 1. Las Vegas, Nevada: Bechtel SAIC Company. ACC: DOC.20040915.0010; DOC.20050419.0001; DOC.20051130.0002; DOC.20060731.0005; LLR.20080311.0066.

Carranza-Torres, C. and Fairhurst, C. 1999. "The Elasto-Plastic Response of Underground Excavations in Rock Masses That Satisfy the Hoek-Brown Failure Criterion." *International Journal of Rock Mechanics and Mining Science, 36,* 777-809. New York, New York: Pergamon. TIC: 256964.

Damjanac, B.; Board, M.; Lin, M.; Kicker, D.; and Leem, J. 2007. "Mechanical Degradation of Emplacement Drifts at Yucca Mountain—A Modeling Case Study. Part II: Lithophysal Rock." *International Journal of Rock Mechanics and Mining Sciences, 44,* (3), 368-399. New York, New York: Elsevier. TIC: 260304.

Hoek, E.; Kaiser, P.K.; and Bawden, W.F. 2000. *Support of Underground Excavations in Hard Rock.* Rotterdam, The Netherlands: A.A. Balkema. TIC: 252991.

Jaeger, J.C. and Cook, N.G.W. 1979. *Fundamentals of Rock Mechanics.* 3rd Edition. New York, New York: Chapman and Hall. TIC: 218325.

Kaiser, P.K.; Diederichs, M.S.; Martin, D.; Sharpe, J. and Steiner, W. 2000. "Invited Keynote: Underground Works in Hard Rock Tunnelling and Mining." *GeoEng2000 International Conference on Geotechnical & Geological Engineering.* Lancaster, PA: Technomic. TIC: 254732.

Lin, M.; Kicker, D.; Damjanac, B.; Board, M.; and Karakouzian, M. 2007. "Mechanical Degradation of Emplacement Drifts at Yucca Mountain—A Modeling Case Study—Part I: Nonlithophysal Rock." *International Journal of Rock Mechanics and Mining Sciences*, *44,* (3), 351–367. New York, New York: Elsevier.

Lorig, L.J. and Cundall, P.A. 1987. "Modeling of Reinforced Concrete Using the Distinct Element Method." *SEM/RILEM International Conference on Fracture of Concrete and Rock, Houston, Texas, June 17-19, 1987.* Shah, S.P. and Swartz, S.E., eds. Pages 459-471. Bethel, Connecticut: Society for Experimental Mechanics. TIC: 260305.

Martin, C.D. 1997. "Seventeenth Canadian Geotechnical Colloquium: The Effect of Cohesion Loss and Stress Path on Brittle Rock Strength." *Canadian Geotechnical Journal, 34,* (5), 698-725. Ottawa, Ontario, Canada: NRC Research Press. TIC: 260303.

Martin, C.D.; Kaiser, P.K.; and McCreath, D.R. 1999. "Hoek-Brown Parameters for Predicting the Depth of Brittle Failure Around Tunnels." *Canadian Geotechnical Journal, 36,* (1), 136-151. Ottawa, Ontario, Canada: NRC Research Press. TIC: 260302.

Mawdesley, C. A. 2002. *Predicting Rock Mass Cavability in Block Caving Mines.* Degree of Doctor of Philosophy. Queensland, Australia: Julius Kruttschnitt Mineral Research Centre – B.Eng (Geol) (Hons).

Plesha, M.E. and Airfantis, E.C. 1983. "On the Modeling of Rocks with Microstructure." *24th U.S. Symposium on Rock Mechanics.* Hougton, MI: Department of Mechanical Engineering and Engineering Mechanics Michigan Technological University.

SNL (Sandia National Laboratories) 2008. *Postclosure Analysis of the Range of Design Thermal Loadings.* ANL-NBS-HS-000057 REV 00. Las Vegas, Nevada: Sandia National Laboratories. ACC: DOC.20080121.0002; LLR.20080408.0251; DOC.20080828.0006.

RAI Volume 3, Chapter 2.2.1.2.1, Number 1

Provide a technical basis for the key assumptions used in the numerical model for estimating the extent and timing of drift degradation due to thermal loading or time-dependent rock weakening. This basis should evaluate how the following assumptions could affect the model results with respect to rock spalling: (i) the simulated rock mass can only fail along randomly oriented surfaces; (ii) blocks behave elastically and therefore a potential fracture cannot propagate through a block; and (iii) the selection of block sizes and size distributions does not bias results against spalling. The technical basis should demonstrate that the assumptions do not lead to results that underestimate the quantity of potential rubble accumulation on and around the engineered barriers. Also, the justification should explain how uncertainties in important parameters are evaluated in the model. This information is needed to verify compliance with 10 CFR 63.114 (e), (f), (g).

1. RESPONSE

In the analysis of the stability of the emplacement drift when subject to thermally induced stresses and time-dependent rock weakening, documented in *Drift Degradation Analysis* (BSC 2004, [DN2002143780/DN2002140376/DN2002203028/ DN2002293941/DEN001579853]), the lithophysal rock mass is represented as a two-dimensional assembly of convex polygonal elastic blocks ("Voronoi blocks") joined along interfaces that can slip or open as a function of stress. To ensure that the behavior of the assembly of Voronoi blocks is mechanically equivalent to the lithophysal rock mass, the micro-properties of the blocks and their interfaces were calibrated to the important mechanical properties (i.e., strength and stiffness) of the lithophysal rock mass as measured in the laboratory. More details of the Voronoi block approach for representation of the rock mass and its calibration can be found in Sections 6.4.2.1 and 7.6.4 of *Drift Degradation Analysis* (BSC 2004).

The following key assumptions are used in construction of the Voronoi block model. The average Voronoi block size (cross-wise linear dimension) is 0.3 m in the analysis presented in *Drift Degradation Analysis* (BSC 2004, Section 6.4.2.1) . The blocks are relatively uniform in size, with a ratio between the minimum and the maximum block size of approximately 2. One feature of Voronoi block geometry is that joints between blocks are oriented randomly. This means that, at any joint intersection, the joints divide the plane in roughly equal angles and there are typically more than three joints per intersection. Consequently, the Voronoi block model simulates an isotropic material if there is no anisotropy in joint mechanical properties, which is the case for the simulations documented in *Drift Degradation Analysis* (BSC 2004).

In RAI 3.2.2.1.2.1-001, the NRC asks: "…how the following assumptions could affect the model results with respect to rock spalling: (i) the simulated rock mass can only fail along randomly oriented surfaces; (ii) blocks behave elastically and therefore a potential fracture cannot propagate through a block; and (iii) the selection of block sizes and size distributions does not bias results against spalling. The technical basis should demonstrate that the assumptions do not lead to results that underestimate the quantity of potential rubble accumulation on and around the engineered barriers." The responses to specific questions are provided in the following text. The first two questions are closely related, because a "rock mass can only fail along randomly oriented surfaces" as "blocks behave elastically and therefore a potential fracture cannot propagate through a block." Therefore, those two questions are addressed jointly.

RAI 3.2.2.1.2.1-001 involves "the extent and timing of drift degradation due to thermal loading or time-dependent rock weakening." The focus in this response is on thermal loading, rather than time-dependent rock weakening. If these calculations were performed with the combined thermal loading and time-dependent strength degradation of the rock mass, the conclusions for RAI 3.2.2.1.2.1-001 are expected to remain unchanged, based on the computational experience described in *Drift Degradation Analysis* (BSC 2004, Appendix S). RAI 3.2.2.1.2.1-002 provides separate responses to the NRC questions on time-dependent rock weakening.

1.1 BLOCK BEHAVIOR AND SIMULATED ROCK MASS FAILURE

The lithophysal rock mass is highly fractured. In the lower lithophysal (Tptpll), abundant short-length fractures (less than 1-m trace length), which connect and intersect lithophysae (accounting for up to 30% of the porosity), create a highly fractured rock mass with ubiquitous fracture fabric (e.g., BSC 2004, Figures 6-10b and 7-1a). Because of relatively short trace lengths, there are abundant solid rock bridges between closely spaced joints such that the bridges must be broken for the rock to fail. Although joint mapping indicates primary vertical joint orientation (BSC 2004, Section 6.1.4.1), the joints combined with lithophysal holes form a generally isotropic ground mass in the lower lithophysal unit (Tptpll), as can be observed on the large-diameter cores taken from this rock (see BSC 2004, Figure 7-1a). The upper lithophysal unit (Tptpul), which is less fractured than the lower lithophysal (Tptpll, Figure 6-10a compared to Figure 6-10b of BSC 2004 [DIRS 166107]), is also a relatively isotropic rock mass because the lithophysae are relatively uniformly distributed. The Voronoi block model does not directly represent the internal structure of the lithophysal rock mass (i.e., fractures and lithophysal holes on the scale of 10 cm). However, on the drift scale, the Voronoi block model is calibrated to behave mechanically equivalent to the lithophysal rock mass (e.g., it has the same stiffness and strength). Randomly oriented joints in the Voronoi block model represent the generally isotropic nature of a lithophysal rock mass and the random fabric created by intense fracturing and lithophysal porosity (e.g., as described in Price 2004, Section 5.2.1.2.3).

As a fracture propagates through the Voronoi block model (i.e., the bonds between the blocks break either in shear or in tension), random joint orientation allows the fracture to develop along a trajectory dictated by the stresses. The trajectory will not be perfectly smooth due to finite block size and the fact that the blocks are elastic (i.e., cannot fracture). This is consistent with the *in situ* observation that fractures in a rock mass are rarely smooth. The reason for this is the typical inhomogeneity of the rock mass on different scales. The fractures will propagate preferentially along planes of weakness, such as grain boundaries or along preexisting joints, because the strength of those planes of weakness or joints can be up to orders of magnitude smaller than the strength of the grains themselves or the strength of small-scale intact rocks. In these circumstances, the grains or the intact blocks between the joints behave elastically. The elasticity of the Voronoi blocks and the fact that in this model the rock mass can fail along the block boundaries accurately reflects the internal length scale of the lithophysal rock mass and the size effect on rock strength. However, macroscopically, as in the case of a homogeneous continuum, the overall path along the block interfaces will tend to "seek" a condition of minimum potential energy. Hence, the overall fracture path in the Voronoi model is not likely to deviate substantially from the "idealized condition" of fracture propagation in a homogeneous continuum with a similar applied stress field.

In the case of the lower lithophysal (Tptpll) rock mass, which is typically highly jointed, it is expected that failure and disintegration of the rock mass will occur preferentially by deformation and extension of the preexisting joints and lithophysae — not by fracturing of intact blocks ("spalling") between those features. This mechanism is corroborated further by Hoek et al. (2000, Section 10.1, which discusses progressive spalling in massive brittle rock, where they state:

> In all cases [when spalling occurs] the rock surrounding the excavation is brittle and massive. In this context massive means that there are very few discontinuities such as joints or, alternatively, the spacing between the discontinuities is of the same order of magnitude as the dimensions of the opening.

Clearly, the lithophysal rock mass is not massive and will not be prone to progressive spalling. The main mode of inelastic deformation will be movement along, and extension of, the preexisting joints and deformation of lithophysal voids.

The potential for stress-related fracture and breakage of small blocks between preexisting fractures can be quantitatively assessed by a simple analysis. For example, the maximum thermally induced stress in the crown of the emplacement drift in lithophysal rock mass Category 5 (which is the stiffest lithophysal unit, and thermally induced stress concentrations will be the greatest) is approximately 45 MPa, as estimated from the stress paths in Figure 6-144 of *Drift Degradation Analysis* (BSC 2004). This thermally-induced stress exceeds the unconfined compressive strength, 30 MPa (BSC 2004, Table 6-41), of Category 5 lithophysal rock mass. However, the rock and rock mass strength manifest a size effect. The strength of intact rock is greater than the strength of the rock mass because joints and, in this case, lithophysae degrade intact rock strength. Furthermore, even the intact (without joints) rock strength increases with reduction in the block size (Hoek and Brown 1982, Figure 69). Because the intact lithophysal rock is lithologically and mechanically similar to, or the same as, the intact nonlithphysal rock mass (see the introductory paragraph of Sections 6.1.4.2 and 7.3.2, page 7-9 of BSC 2004), the strength and size effect of intact lithophysal rock are deduced from test data on the nonlithophysal rock. This is a reasonable approach because the different mechanical characteristics of the lithophysal versus nonlithophysal rock masses are caused by the different internal structure, not due to intact rock properties.

The strength of the intact tuff (without major joints or lithophysae) on blocks 100 mm through 300 mm in size (i.e., the size of the Voronoi blocks in the lithophysal model) is estimated to be between 85 and 109 MPa (the equation in BSC 2004, Figure E-22). The thermally induced stresses in the rock are less than 45 MPa, which is about 53% of the minimum intact rock strength of 85 MPa. It follows that fracturing of the lithophysal rock mass will occur as a consequence of movement and extension along the preexisting joints, not by fracturing of the small intact blocks or spalling.

The failure mode for the nonlithophysal rock mass can differ from the lithophysal rock mass. For example, the maximum tangential stress in the drift crown during the drift-scale heated experiment was in excess of 90 MPa, as shown in Figure 7-34 of *Drift Degradation Analysis* (BSC 2004), and that stress caused rock spalling, as was observed during the experiment. The predicted thermally induced stresses in the crown of the drift-scale heated experiment are approximately two times greater than the predicted stresses in the crown of the emplacement drift because of: (1) greater temperature during the heated-drift experiment than around the emplacement drifts and (2) greater stiffness of the nonlithophysal rock mass than that of the lithophysal rock mass. The drift scale heater experiment is in nonlithophysal rock with widely spaced fractures, so spalling is a potential failure mechanism during this test, as explained in Section 2.1 of Response to RAI Introduction.

Although the Voronoi blocks do not directly represent the joints and lithophysae of the lithophysal rock mass, the Voronoi block size of 300 mm is consistent with the approximate block size created in lower lithophysal (Tptpll) rock mass by joints and lithophysae. (see additional discussion in Section 1.2, including sensitivity analysis of block sizes between 100 and 300 mm.) For thermally induced stresses, the main mode of lithophysal rock mass failure will be slip, opening and extension of preexisting joints, not fracturing of the blocks between the joints. Consequently, the assumptions that: (1) the Voronoi block model can fail only along randomly oriented surfaces, and (2) the blocks between those surfaces are elastic, are justified and consistent with actual behavior of the lithophysal rock mass.

1.2 SELECTION OF BLOCK SIZES AND SIZE DISTRIBUTIONS DOES NOT BIAS RESULTS AGAINST SPALLING

As presented in *Drift Degradation Analysis* (BSC 2004), the average Voronoi block size of 300 mm used in the calculations for drift stability in the lithophysal rock mass was selected to be representative of the actual block size created in the lithophysal rock mass by the preexisting jointing and lithophysae (BSC 2004, Section 6.4.2.1). An exact estimate of the actual block size is difficult. Although the average joint spacing is of the order of 100 mm (BSC 2004, Section 6.1.4.1), some of the joints are not actual discontinuities. As can be seen from Figure 7-1a of *Drift Degradation Analysis* (BSC 2004), a number of “joints” have sufficient strength (i.e., cohesion and tensile strength) to allow recovery of samples that are ~0.5-m long.

It was decided to carry out the analysis documented in *Drift Degradation Analysis* (BSC 2004) with an average block size of 300 mm because this size is representative of the internal discontinuities of the rock mass. As shown in Equation 1-1, this block size, l_B, is also much smaller than the characteristic length scale of the model, the drift diameter, D:

$$(l_B / D) = 0.055 << 1 \qquad \text{(Eq. 1-1)}$$

which is the necessary condition to ensure that the block size does not affect the modeling results. Furthermore, in the simulations for *Drift Degradation Analysis* (BSC 2004), drift stability for the thermally induced stress was analyzed for different realizations of the Voronoi block geometry (but using the same average block size) (DTN: MO0408MWDDDMIO.002). The fact that the results were not sensitive to change in the block geometry realization is another indication that the block size does not affect the results.

To further demonstrate the insensitivity of the modeling results to block size, additional simulations (not documented in BSC 2004) of drift stability were conducted with average Voronoi block sizes of 0.2 and 0.1 m (SNL 2009). These additional simulations were performed for rock mass Categories 2 and 5, based on thermally induced stresses during the first 10,000 years after repository closure. The predicted drift configurations after 10,000 years are shown in Figures 1-1 and 1-2. None of the cases indicates any consequential rockfall. (A small unraveling can be observed from the drift walls in Category 2 for block sizes of 0.2 and 0.1 m). The new results for 0.2- and 0.1-m block sizes are consistent with the results for the 0.3-m block size, documented in Section 6.4.2.3.1 and Figure 6-140 of *Drift Degradation Analysis* (BSC 2004). Because the results of the thermal analysis, which indicate fracturing of the rock mass, are insensitive to the change in the block size from 0.3 to 0.1 m, and because the analysis of the drift stability for thermal loading and time-dependent strength degradation (BSC 2004, Figures S-42 to S-44) for 0.3-m block size show relatively small amount of the rockfall, the results of that analysis too are expected to be insensitive to the change in block size from 0.3 to 0.1 m. Thus, the drift degradation model results are not expected to be affected by the change in block size from 0.3 to 0.1 m. The block size distribution (or range between the largest and the smallest block) is not significant when the block size is sufficiently small, as demonstrated here.

Figure 1-3 shows in detail the stresses and damage in the drift crown after 100 years of heating predicted in the model with 0.1-m block size. The stresses have initiated fractures subparallel to the drift crown, which did not result in rockfall. Instead, the regions along the drift wall are destressed, while large stress concentrations are “pushed” deeper into the rock. The presence of large stress concentrations deeper in the rock mass does not result in additional fracturing because there is a corresponding increase in the confining stress away from the excavation.

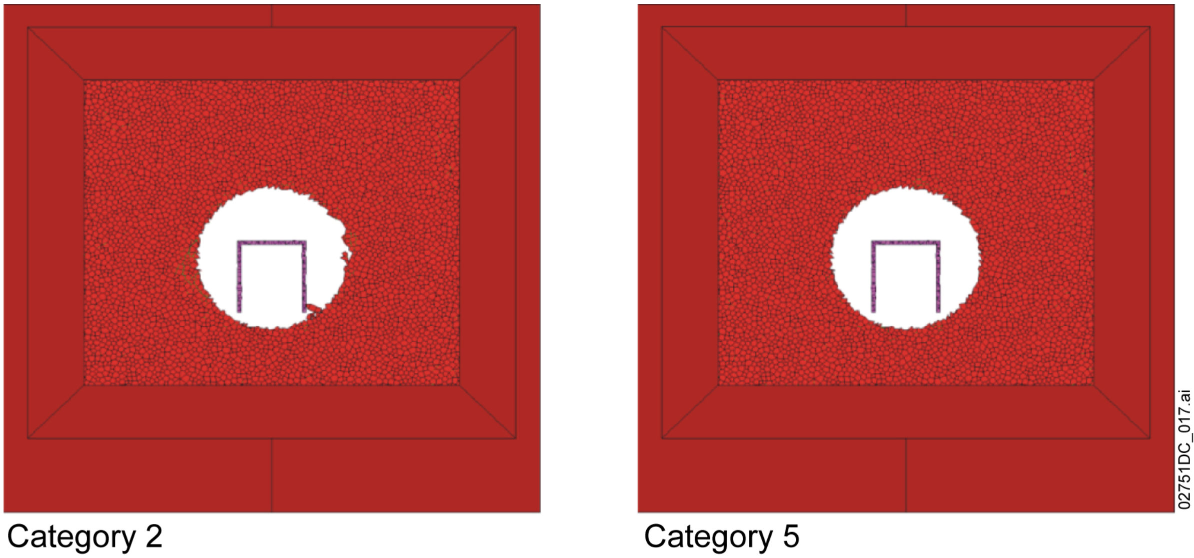

Source: SNL 2009, Figure 4-1.

Figure 1-1. Predicted Drift Profiles with 0.2-m Voronoi Block Size due to Thermal Load 10,000 years after Waste Emplacement

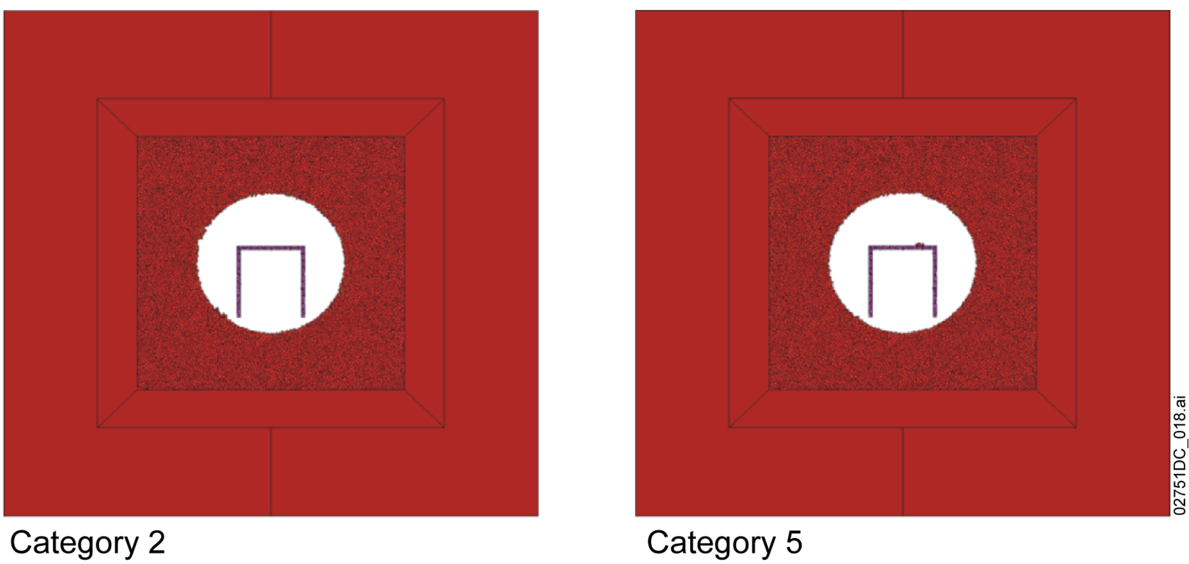

Source: SNL 2009, Figure 4-2.

Figure 1-2. Predicted Drift Profiles with 0.1-m Voronoi Block Size due to Thermal Load 10,000 years after Waste Emplacement

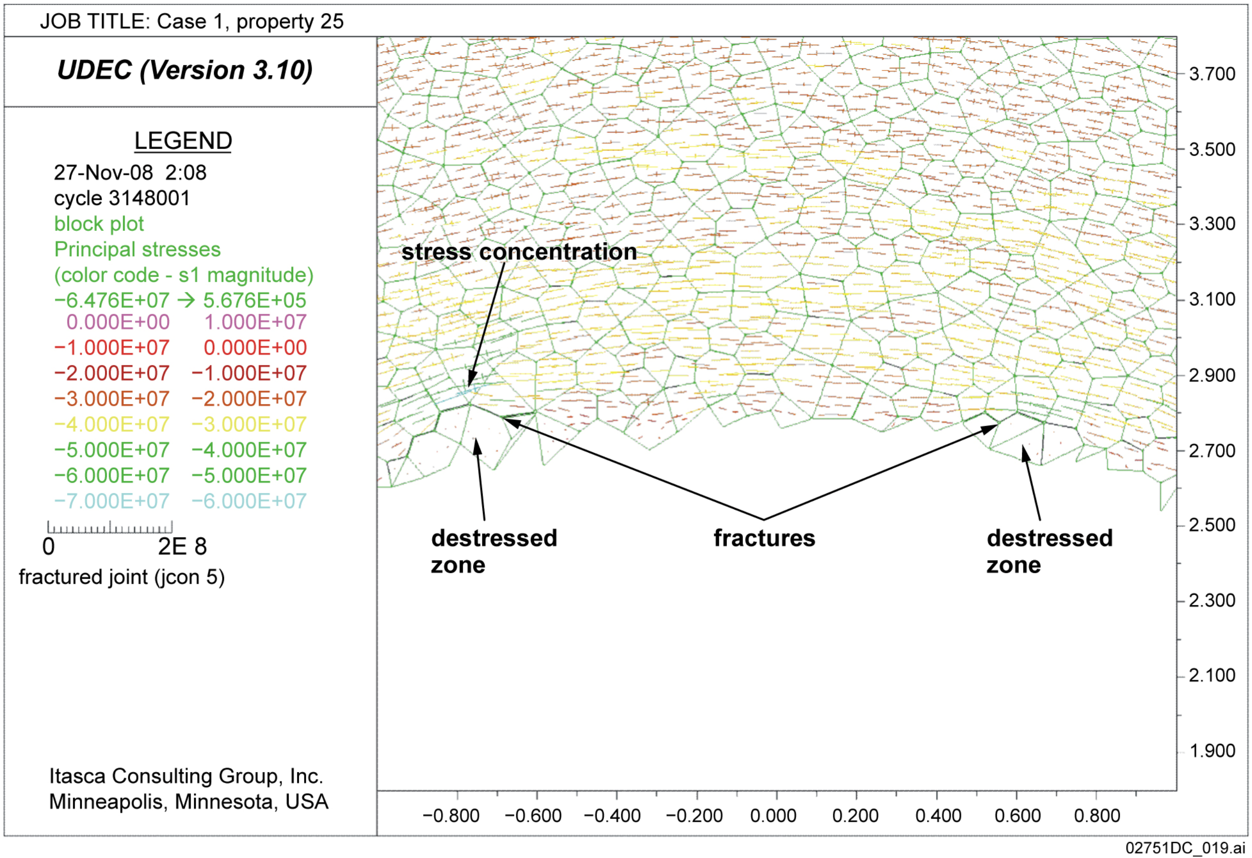

NOTE: Locations of micro-cracks, or locations where contacts between the blocks have failed, are indicated by black lines. Compressive stresses are negative.

Source: SNL 2009, Figure 4-3.

Figure 1-3. Detail of Drift Crown, with Stress Tensor Field (Pa) Colored by Magnitude of the Major Principal Stress, After 100 Years of Heating as Predicted by the Model with 0.1-m Voronoi Block Size

1.3 EVALUATING IMPORTANT PARAMETER UNCERTAINTIES

The most important parameters affecting the drift stability in the lithophysal units are the mechanical properties (i.e., stiffness and strength) of the rock mass and the loading conditions. For example, thermally induced stresses are proportional to the rock mass stiffness; onset of yielding of the rock mass is defined by the rock mass strength. Uncertainty in time-dependency of rock mass strength is discussed in response to RAI 3.2.2.1.2.1-002 (00058-00-00). The greatest stresses induced in the rock mass under a nominal scenario are due to heating of the rock mass. Evaluation of uncertainties in rock mass quality and thermal loading is discussed in this section.

Variability of the lithophysal rock-mass quality is represented in the analysis by five rock-mass categories, from Category 1 (for unconfined compressive strength of 10 MPa) to Category 5 (for unconfined compressive strength of 30 MPa). As indicated in Table E-10 of *Drift Degradation*

Analysis (BSC 2004), there is a good correlation between the lithophysal porosity and the rock mass quality.

Drift degradation calculations were carried out for all five lithophysal rock mass categories. In the calculations, it was assumed that a selected rock-mass category is uniform throughout the two-dimensional cross-section of a drift. This assumption led to representation of more extreme conditions in the model than those that could be estimated from the statistical model of spatial distribution of lithophysal porosity (e.g., BSC 2004, Figure E-15). Considering the spatial variability of the lithophysal porosity relative to the drift and model size, it is clear that extreme values of lithophysal porosity and, particularly, rock mass Category 1 with porosity greater than 30%, are localized. Thus, assuming homogeneous properties throughout the two-dimensional model domain for the extreme rock-mass qualities (categories 1 and 5) results in bounding of the drift response with respect to variability of lithophysal rock-mass quality. Furthermore, as discussed in Section S4 of *Drift Degradation Analysis* (BSC 2004), stability of the drifts was also analyzed considering the distribution of lithophysal porosity in the ECRB Cross-Drift and correlation between porosity and the rock mass quality (BSC 2004, Figure S-50).

Sensitivity of the drift stability to variability in the range of thermal loading was investigated and the results reported in *Postclosure Analysis of the Range of Design Thermal Loadings* (SNL 2008 [DEN001573236/DEN001592171/DEN001601447]). The analysis and the results for the two highest temperature cases are documented in detail in Section 6.4.1 of that report (SNL 2008). The following two cases were considered:

> Case 1 – The maximum effective local-average thermal line load (the 7-package average of the 7-point segment from the 96/2 emplacement sequence)
>
> Case 2 – An extreme local-average line load for sensitivity testing (the 3-package average of the 3-point. hottest segment from the 96/2 sequence).

The maximum drift-wall temperatures for Cases 1 and 2 were approximately 200°C and 340°C, respectively, (SNL 2008, Figure 6.4.1-1), compared to approximately 140°C in the nominal case (BSC 2004, Figure 6-26). Cases 1 and 2 have been analyzed for lithophysal rock-mass Categories 1, 3 and 5. Results for Cases 1 and 2 show thermally induced rockfall greater than that predicted for the nominal case because the maximum drift-wall temperatures are greater than 140°C. For example, the drift configuration after 95 years and 1,000 years in the Category 3 lithophysal rock mass for Case 1 (200°C maximum temperature) is shown in Figure 1-4.

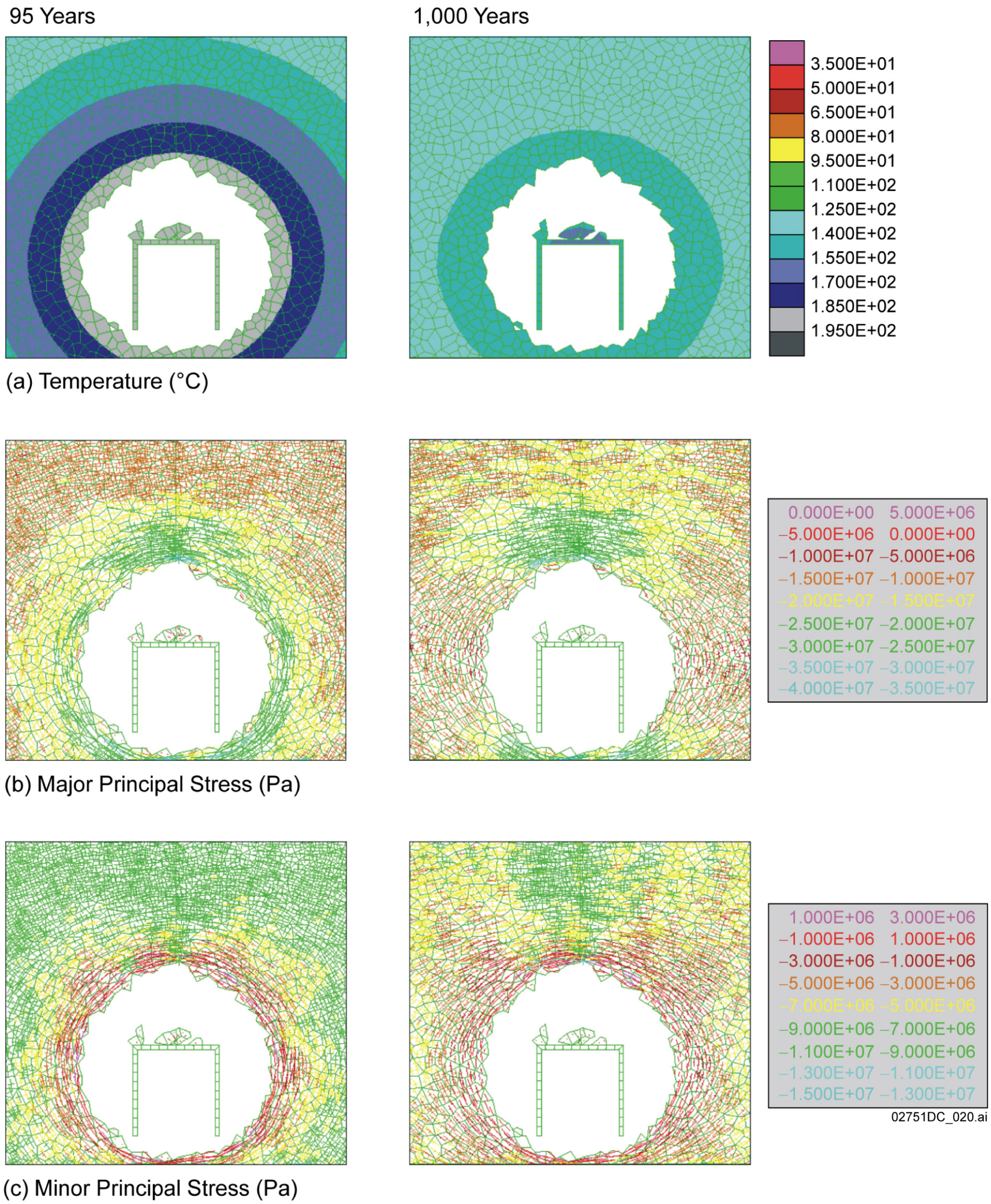

Source: SNL 2008, Figure 6.4.1-5.

Figure 1-4. Drift Configuration, Temperatures and Stresses for Case 1 of Thermal Load, Category 3 Lithophysal Rock Mass

The increase in maximum temperature causes minor rockfall from the drift crown, forming a notch, approximately 0.5-m deep, but the rock mass reaches a stable equilibrium configuration because the stress concentrations move deeper into the rock, where the confining stress is greater. There is no evidence of progressive spalling from the crown where high stress concentrations occur.

This model does not account for the effects of the changes in drift configuration and rubble accumulation on heat transfer to and temperature field in the rock mass. In other words, the temperature field is calculated assuming that the initial drift configuration does not change, irrespective of the rockfall volume and associated change in drift profile. However, the change in temperature field due to notch formation is modest in Case 1, because the maximum temperature change at the notch tip is estimated to be approximately 10°C for the predicted drift configurations. (The interval between the temperature contour lines in Figure 1-4 is 15°C. The drift profile advance as a result of rockfall is much less than the spacing of the temperature contours lines even at 95 years. Assuming that the temperature at the notch tip would increase to the same temperature as that on the drift wall surface if the rockfall did not occur, the temperature change is estimated to be 10°C—the difference between the temperature on the drift surface and the temperature at the location of the notch tip.) The maximum stress change due to temperature change can be estimated using the formula (BSC 2004, Section 6.2, Equation 6-6) for the mean stress change under confined conditions:

$$\begin{aligned} \Delta\sigma_{ij} &= 3\delta_{ij} K \alpha \Delta T \\ \Delta\sigma &= 3 \times 6.01 \times 10^{3} \times 9.07 \times 10^{-6} \times 10 = 1.6 \text{ MPa} \end{aligned} \quad \text{(Eq. 1-2)}$$

where $K = 6.01 \times 10^{3}$ MPa is the bulk modulus for Category 3 rock mass (BSC 2004, Table E-10), $\alpha = 9.07 \times 10^{-6}\ 1/^{\circ}\mathrm{C}$ is the thermal expansion coefficient for tuff for the temperature range $100^{\circ}\mathrm{C} < T \le 125^{\circ}\mathrm{C}$ (BSC 2004, Table E-20), and $\Delta T = 10^{\circ}\mathrm{C}$ is the approximated temperature change due to profile change. [δ_{ij} is the Kronecker delta symbol. The value of 1 for diagonal term is taken for the calculation in Equation 1-2.] The estimated stress change of 1.6 MPa is approximately 5% of the maximum stress (~30 MPa) in Figure 1-4 and, thus, is inconsequential for drift stability.

1.4 ASSUMPTIONS DO NOT LEAD TO RESULTS THAT UNDERESTIMATE POTENTIAL RUBBLE ACCUMULATION ON AND AROUND THE ENGINEERED BARRIERS

The use of the UDEC model to predict rubble accumulation does not underestimate the quantity of rubble that might accumulate on and around the engineered barriers. The assumptions that: (1) the Voronoi block model can fail only along randomly oriented surfaces, and (2) the individual blocks are elastic, are justified and consistent with the actual behavior of the lithophysal rock mass, as explained in Section 1.1 of this response. The results from the UDEC model for drift degradation are not affected by the change in block size from 0.3 m to 0.2 m or 0.1 m, as explained in Section 1.2 of this response. It follows that the block size distribution (or range between the largest and the smallest block) is not significant when the block size is sufficiently small. Finally, the block size does not need to be small compared to potential spalling zones because spalling occurs in massive rock units with widely separated discontinuities and the lithophysal units are not massive because of the closely spaced fractures and lithophysae. The assumptions in the UDEC representation of lithophysal response do not underestimate the volume of rubble. In addition, the UDEC predictions of rockfall volume are consistent with the observed rockfall volume from the Drift Scale Heater Test, as shown in the response to RAI 3.2.2.1.2.1-006 (00062-00-00).

2. COMMITMENTS TO NRC

None.

3. DESCRIPTION OF PROPOSED LA CHANGE

None.

4. REFERENCES

BSC (Bechtel SAIC Company) 2004. *Drift Degradation Analysis*. ANL-EBS-MD-000027 REV 03. Las Vegas, Nevada: Bechtel SAIC Company. ACC: DOC.20040915.0010; DOC.20050419.0001; DOC.20051130.0002; DOC.20060731.0005; LLR.20080311.0066.

Hoek, E. and Brown, E.T. 1982. *Underground Excavations in Rock*. London, England: The Institution of Mining and Metallurgy. TIC: 217577.

Hoek, E.; Kaiser, P.K.; and Bawden, W.F. 2000. *Support of Underground Excavations in Hard Rock*. Rotterdam, The Netherlands: A.A. Balkema. TIC: 252991.

MO0408MWDDDMIO.002. Drift Degradation Model Inputs and Outputs. Submittal date: 11/26/2008.

Price, R.H. 2004. *The Mechanical Properties of Lithophysal Tuff: Laboratory Experiments.* TDR-EBS-MD-000027 REV 00. Las Vegas, Nevada: Bechtel SAIC Company. ACC: DOC.20040506.0001.

SNL (Sandia National Laboratories) 2008. *Postclosure Analysis of the Range of Design Thermal Loadings*. ANL-NBS-HS-000057 REV 00. Las Vegas, Nevada: Sandia National Laboratories. ACC: DOC.20080121.0002; LLR.20080408.0251; DOC.20080828.0006.

SNL 2009. *Supplemental Rockfall Analyses for RAI 3.2.2.1.2.1-001 and RAI 3.2.2.1.2.1-006*. PARD-MGR-DE-000231 REV 00. Las Vegas, Nevada: Sandia National Laboratories. ACC: LLR.20090122.0086. (Provided as Enclosure 8.)

RAI: Volume 3, Chapter 2.2.1.2.1, Number 2

Provide the technical basis for assuming a linear relationship fit to represent the time-to-failure versus stress-ratio data for tuff (Safety Analysis Report Figure 2.3.4-44; Bechtel SAIC Company, 2004, Figures 6-155 and S-2). The basis should explain how the linear fit accounts for uncertainties in time-to-failure of rock subjected to sustained loading, including results of numerical model calculations described in Section S2.2 of Bechtel SAIC Company (2004). The basis should also explain how uncertainty in the mathematical fit was evaluated. This information is needed to verify compliance with 10 CFR 63.114 (c), (e), (f).

1. RESPONSE

1.1 INTRODUCTION

The most relevant data on the time-dependent behavior of the lithophysal rock mass and its effect on drift degradation are approximately 10 years of observations of the behavior of the 7.62-m diameter Exploratory Studies Facility (ESF) and the 5-m diameter Enhanced Characterization of the Repository Block (ECRB) Cross-Drift since their excavation. The ESF and ECRB Cross-Drift are similar in size to the emplacement drifts (5.5 m in diameter). The elastically calculated stress concentrations in the drift wall, which are approximately 17.5 MPa (see response to RAI 3.2.2.1.2.1-003), is between 58% (rock mass Category 5) and more than 100% (rock mass Category 2) of the short-term unconfined compressive strength of the lithophysal rock mass (BSC 2004, Table E-10). (The ratio of the stress to the short-term strength is usually called the driving-stress ratio.)

The ESF and ECRB Cross-Drift were excavated more than 10 years ago and are lightly supported in the crown only. There is no support at the springline, where the in situ stress concentrations and driving-stress ratios are greatest. Consequently, the ground support has no effect on potential time-dependent drift deterioration. Thus, the ESF and the ECRB Cross-Drift are large-scale experiments on time-dependent behavior of lithophysal rock for the relevant range of driving-stress ratios (between 0.58 and 1.0, depending on rock mass quality), and for a longer time (10 years) than is available from any laboratory experiments. Thus, the observations of drift behavior are significant in the evaluation of the representativeness of the numerical model used to evaluate time-dependent drift stability.

The ESF and ECRB Cross-Drift are in excellent condition. There are no observations on the drift walls or crown of stress-induced fracturing or of any kind of deterioration either immediately after excavation or during the time since the excavation, irrespective of the lithophysal porosity or rock mass quality. A significant number of 12-inch diameter diamond drill boreholes for large-core sampling were drilled in the sidewalls and the shoulders of the ESF and ECRB tunnels at various locations within the lower and upper lithophysal units. Inspection of the holes' walls immediately after drilling showed stress-induced fracturing in one hole, which was drilled in rock mass Category 1 (highest porosity) rock in the ESF (BSC 2004, Figure 7-25). All other holes showed no signs of sidewall fracturing. Subsequent inspections did not show additional fracturing in any of the holes. All of these observations confirm that drifts excavated in the lithophysal rock exhibit very little or no time-dependent strength degradation for a period of 10 years.

There is relatively high uncertainty in the available laboratory data on time-dependent strength degradation of the tuff (e.g., BSC 2004, Figure 6-155). In the numerical modeling, the tuff data are approximated with a linear fit in a plot of logarithm of time-to-failure versus the driving-stress ratio, for driving-stress ratios between 0 and 1. As discussed in the following text, the technical basis for the linear fit for the high values of the driving-stress ratio are the linear relationships observed from the fundamental study of stress-corrosion mechanisms on quartz (Scholz 1972; Martin et al. 1997) and extensive laboratory testing data on Lac du Bonnet granite (Schmidtke and Lajtai 1985; BSC 2004, Figure 6-155).

The linear fit clearly underestimates the time-to-failure for low driving-stress ratios because the long-term strength of rocks is typically in the range between 0.4 and 0.6 of the short-term strength (Lama and Vutukuri 1978, Volume III, Section 9.10), implying that a time-to-failure curve must be asymptotic to a vertical line at driving stress ratio between 0.4 and 0.6. The uncertainty in the data and its approximation by the linear fit for driving-stress ratios greater than 0.6 were addressed by calibrating the model results with respect to observation of the behavior of the ESF and the ECRB Cross-Drift. The best-fit tuff linear approximation (i.e., the mean curve) of time-to-failure, used in the numerical simulation of drift stability under in situ stress conditions (BSC 2004, Figures S-37 and S-39), shows more damage and drift degradation in 10 years than is observed in the ESF and the ECRB Cross-Drift. Thus, the linear fit used in the numerical modeling provides a bounding prediction that over-predicts rockfall and rubble accumulation from time-dependent strength degradation.

1.2 SUMMARY OF TECHNICAL BASIS FOR LINEAR FIT APPROACH

The technical basis for assuming a linear relationship to represent the logarithm of the time-to-failure versus stress-ratio data for tuff (SAR Figure 2.3.4-44; BSC 2004, Figures 6-155 and S-2) is based on information contained in SAR Section 2.3.4.4 and in *Drift Degradation Analysis* (BSC 2004, Sections 6.4.2.4, 6.5, S2.2.4, and S3.2). To briefly summarize:

- The strength of the stressed rock mass exposed to humidity will degrade over time due to a stress corrosion mechanism. The stress corrosion mechanism (described in BSC 2004, Section 6.4.2.4.2) gives rise to a linear relationship of the logarithm of the time-to-failure as a function of the state of stress, the temperature, and the pore pressure (Scholz 1972; Martin et al. 1997) for stresses greater than the stress threshold below which the stress corrosion process is inactive. The relationship between time-to-failure and the state of stress is referred to as a static-fatigue curve. Drift degradation analyses have conservatively represented the static-fatigue curve as a straight line dependence of the logarithm of time-to-failure versus the driving-stress ratio (SAR Section 2.3.4.4.6.1, p. 2.3.4-96; BSC 2004, Section 6.4.2.4.2.2) at all driving-stress ratios. Thus, the linear relation for high driving-stress ratios is based on the stress corrosion mechanism (and confirmed by testing data, e.g., Schmidtke and Lajtai 1985); the linear relation for low driving-stress ratios is a conservative assumption because the time-to-failure curve must be asymptotic to a vertical line at driving-stress ratio between 0.4 and 0.6.

- There is uncertainty in long times-to-failure for low driving-stress ratios because of a lack of data for long times-to-failure. The linear fit to the static-fatigue data accounts for uncertainties in time-to-failure of rock subjected to sustained loading because the straight line under-predicts time-to-failure for low values of the driving stress ratio (BSC 2004, Section 6.5, p. 6-237). Based on data for Lac du Bonnet granite (BSC 2004, Appendix S, Figure S-27, p. S-26), the linear fit for the static-fatigue curve underestimates time-to-failure compared to experimental data in the range of driving-stress ratios between 0.65 and 0.70 (which corresponds to the longest measured times-to-failure). A linear fit provides a representation of the static-fatigue data for computer modeling studies that over-predicts rockfall, as explained in Section 1.3.2 of this response.

- Uncertainty in the mathematical fit of the data was evaluated using the coefficient of determination, which is a measure of how well the linear fit approximates the actual data (BSC 2004, Figure 6-155, p. 6-203). The coefficients of determination are 0.738 and 0.7801 for the Lac du Bonnet granite data and the 1997 tuff data, respectively, providing a very reasonable representation of these data sets. There is considerably more scatter for all the tuff data, with a coefficient of determination of 0.4822, although the linear fits to the two tuff data sets (1997 alone or 1997 and 2004) show the consistency of the overall slope of the fits.

- Various linear fits to laboratory data from both tuff and Lac du Bonnet granite were applied to the UDEC rockfall model to compare model performance to field conditions in the ESF (BSC 2004, Sections S3.2 and S3.4.1, pp. S-25 and S-32, respectively). Using the static-fatigue curves for Lac du Bonnet granite, the model predictions after 5 and 10 years for rock mass Categories 1 and 2 show significant amounts of rockfall and some degradation at the springline for rock mass Category 5 (BSC 2004, Figures S-33 through S-35). These results are in disagreement with over 10 years of observations in the ESF and ECRB, which are stable with no observations of degradation with time. The static-fatigue curves for Lac du Bonnet granite result in too rapid deterioration of the drift, and do not provide a good representation of time-dependent behavior of the lithophysal tuff (BSC 2004, Section S3.4.1, p. S-34).

  The linear fits to the static-fatigue data for tuff, on the other hand, produce better agreement of the UDEC model predictions with observations of tunnel performance, although even in this case there is more fracturing and rockfall after 10 years than observed underground (BSC 2004, Figures S-37 and S-38). The tuff best-fit static-fatigue lines are in best agreement with both observations of tunnel performance and the results from short-term tests on the lithophysal rock mass (BSC 2004, Sections S3.4.1 and S6, pp. S-34 and S-60, respectively). Thus, based on comparison between the observations of the behavior of the ESF and the ECRB Cross-Drift over 10 years and the model prediction, the best-fit tuff linear approximation accounts for uncertainties in the data by providing a bounding, conservative estimate of time-dependent strength degradation.

- Case histories of tunnel performance at Yucca Mountain and at Hoover Dam provide additional evidence that unsupported or lightly supported tunnels in moderately to densely welded tuff can stand in a stable condition for several decades with no obvious sign of deterioration (SAR Section 2.3.4.4.6.1, p. 2.3.4-93; BSC 2004, Section 6.4.2.4.1.3, pp. 6-193 to 6-196).

In summary, the approach for assessing the time-dependent strength behavior of rock is based on a linear fit to the data that tends to over-estimate rockfall, as confirmed by comparison of the model predictions with observations of behavior of the ESF and ECRB over a period of 10 years since their excavation. The time-dependent strength behavior of rock is predicted to cause only partial collapse of the drift during the first 10,000 years after repository closure, based on a bounding, conservative estimate of time-dependent strength degradation (BSC 2004, Section 8.1, p. 8-3). Therefore, the uncertainties in time-to-failure of rock have little impact on repository performance.

1.3 DISCUSSION

1.3.1 Theoretical Basis for Linear Fit

The emplacement drifts will be subjected to in situ and slowly changing thermally induced stress conditions over a long time period. To estimate potential long-term failure times and mechanisms in the Topopah Spring Tuff, determination of the time to failure as a function of stress level is necessary.

The relationship of time-to-failure as a function of applied stress level for a rock is typically determined by conducting creep experiments in the laboratory on rock samples at heated and saturated conditions. During a creep experiment, the rock sample is loaded to some percentage of its estimated compressive strength and held constant while the sample strain is monitored. The sample will eventually fail ("static fatigue limit") and the time to failure can be plotted against the ratio of applied stress to rock unconfined compressive strength ("driving-stress ratio") to establish a time-dependent failure condition for the rock. The slope of this plot is indicative of the rate of strength time-dependency (SAR Section 2.3.4.4.6.1, p. 2.3.4-94).

The long-term strength predictions (BSC 2004, Section 6.4.2.4 and Appendix S) are based on limited static-fatigue test data, which provide time-dependent strength behavior of the lithophysal rock. One of the main limitations of the prediction of time-dependent behavior of excavations in a rock mass, for a period of 10 years or longer after excavation, is that existing static-fatigue testing (for any rock) is typically performed for no more than a few months. Predictions for longer time frames are based on extrapolation of existing testing data, and involve a significant level of uncertainty. The static-fatigue curve is usually considered to be a straight line in a plot of the logarithm of time-to-failure versus driving-stress ratio, which is fitted to experimental data. Scholz (1972, Equations 3 and 4) has developed such a relation in his fundamental study of static fatigue of quartz. The mechanism of stress corrosion in quartz and tuff, both of which are brittle materials, is similar and related to magnitude of stress at the fracture tips. Although the stresses in the rock mass are more heterogeneous than in the quartz tested in the laboratory, the average response, particularly for large driving-stress ratios, has the same functional dependence on applied load. Also, the most extensive laboratory data on static fatigue of rock, for Lac du Bonnet granite (Schmidtke and Lajtai 1985; BSC 2004, Figure 6-155), is well approximated by a linear fit in the semi-logarithmic plot.

1.3.2 How the Linear Fit Accounts for Uncertainties at Low Driving-Stress Ratios

The static-fatigue behavior of Lac du Bonnet granite and welded lithophysal tuff forms the basis of the UDEC model for stress corrosion around a drift. The static-fatigue curves provide the time-to-failure of the material at a particular driving-stress ratio.

The static-fatigue data for Lac du Bonnet granite at 0 and 5 MPa confinement, and tuff at 5 MPa confinement and 4.5 MPa pore pressure, are shown in *Drift Degradation Analysis* (BSC 2004, Figure S-2, p. S-6). Each data set was fit with a straight line, and the line was extrapolated to encompass driving-stress ratios ranging from zero to one. This approach will under-predict time-to-failure because the curves most likely approach infinity at a driving-stress ratio approaching zero (i.e., the rocks have long-term or true strength greater than zero; Lama and Vutukuri 1978, Volume III, Section 9.10), as illustrated in Figure 1. It appears from available data for Lac du Bonnet granite (BSC 2004, Appendix S, Figure S-27) that the fitted static-fatigue curve under-estimates time-to-failure compared to experimental data in the range of driving-stress ratios between 0.65 and 0.70 (which corresponds to the longest measured times-to-failure). It seems that a curved line (instead of a straight line) as shown in Figure 1 would be a better fit for long times-to-failure.

Rocks have a long-term strength. If rock is loaded with stress greater than the long-term strength and smaller than short-term strength, it will not fail instantaneously, but will fail eventually within a finite time if the load is maintained. However, if the rock is loaded below the long-term strength, it will never fail irrespective of the duration of the load. Many authors (e.g., Lama and Vutukuri 1978, Volume III, Section 9.10) agree that long-term strength of rock coincides with the crack initiation threshold. The crack initiation threshold for rocks is typically between 0.4 and 0.6 of the short-term rock strength, σ_c (e.g., Lama and Vutukuri 1978, Volume III, Section 9.10; Martin 1997, Figure 3). Existence of the long-term strength of rock, which is at approximately $0.4\sigma_c$ to $0.6\sigma_c$, implies that the time-to-failure line must be asymptotic with the vertical line at $0.4\sigma_c$ to $0.6\sigma_c$. Thus, as indicated in Figure 1, linear extrapolation on the semi-logarithmic plot for static fatigue implies that a rock has zero long-term strength and underestimates the time-to-failure for small driving-stress ratios. Consequently, the linear fit bounds uncertainties in time-to-failure of rock subjected to sustained loading at low driving-stress ratios because the straight line under-predicts time-to-failure for low values of the driving stress.

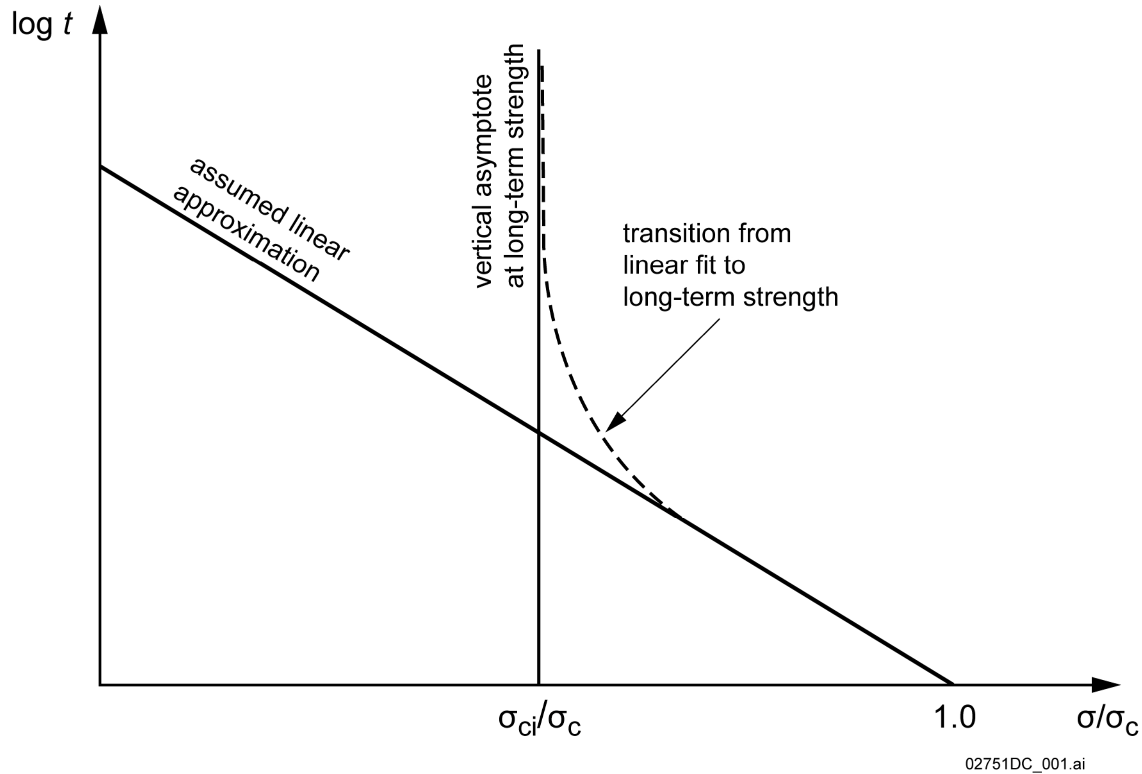

Source: For illustration purposes only.

Figure 1. Illustration of Approximations of Time-to-Failure Curve

1.3.3 Evaluation of Static-Fatigue Curves at High Driving Stress Ratios

Uncertainty in the mathematical fit of the data was evaluated using the coefficient of determination for a regression fit, usually denoted as R^2, which is a measure of how well the linear fit approximates the actual data (BSC 2004, Figure 6-155, p. 6-203). Linear fits to the unconfined compression data of Lac du Bonnet granite and to the 1997 tuff data only and to the welded tuff data (including both 1997 and 2004 data) are given in *Drift Degradation Analysis* (BSC 2004, Figure 6-155, p. 6-203). The coefficients of determination are 0.738 and 0.7801 for the Lac du Bonnet granite and the 1997 tuff data, respectively, providing a very reasonable representation of the data sets. There is considerably more scatter for all the tuff data, with a coefficient of determination of 0.4822, although the linear fits to the tuff data sets (1997 alone or 1997 and 2004) show the consistency of the overall slope of the fits. Due to data uncertainty, a lower bound for the slope of the time-to-failure curve based on the Lac du Bonnet data was also used in numerical modeling estimates.

The sensitivity in the predictions of the UDEC model for drift degradation was evaluated by using the time-dependent strength degradation obtained from Lac du Bonnet granite as a lower bound and by using the linear fit to the data for the time-dependent strength loss of Topopah Spring Tuff as a best estimate. Model prediction for different categories of rock mass quality

(1 through 5), combined with these two fits for static-fatigue, were compared with observations from the ESF and ECRB (BSC 2004, Sections S3.2 and S3.4.1, pp. S-25 and S-32).

The drifts have been open for over 10 years and no indication of any time-dependent deterioration has been observed during this period. The drifts are supported with rock bolts and wire mesh in the roof only. There is no ground support in the walls. The stress state in the wall is approximately 17.5 MPa (see response to RAI 3.2.3.1.2.1-003). That stress level exceeds the short-term strength of lithophysal rock mass Categories 1 and 2 (i.e., 10 MPa and 15 MPa; BSC 2004, Table E-10), but is also 87.5% of the short-term strength for lithophysal rock mass Category 3.

The UDEC model with the tuff best-fit static fatigue curve (i.e., BSC 2004, Figure 6-155) predicts failure (yielding) of the rock mass within hours for a driving-stress ratio of 0.875. Categories 1, 2, and 3 comprise approximately 40% of the lithophysal rock mass on the repository level (BSC 2004, Figure S-50). Although this analysis implies that observations of rock yielding and time-dependent drift deterioration should be widespread within the ESF and ECRB, there is no indication of time-dependent damage or fracturing. A significant number of 12-inch diameter diamond drill boreholes were drilled in the sidewalls and shoulders of the ESF and ECRB at various locations within the lower and upper lithophysal units (BSC 2004, Section 7.6.5.2). Observation in only one hole, drilled in Category 1 (highest porosity) rock in the ESF (BSC 2004, Figure 7-25), showed stress-induced fracturing, parallel to the drift wall to a depth of approximately 0.5 m. Stress-induced fracturing has not been observed in any other hole or anywhere on the drift walls since the drifts were excavated and the holes drilled.

Comparison of the model predictions of drift behavior after 10 years with underground observations led to the following conclusions (BSC 2004, Section S3.4.1): (a) the Lac du Bonnet static-fatigue curve is inconsistent with Yucca Mountain tunnel behavior because it leads to some predicted rockfall after 10 years for all rock mass categories, and (b) the poorest quality rock mass can be represented as rock mass Category 2 with the tuff best-fit static-fatigue curve. Although the tuff best-fit static-fatigue curves over-predict time-dependent strength degradation, they produce the best agreement with both observations of tunnel performance and the results from short-term tests on the lithophysal rock mass (BSC 2004, Sections S3.4.1 and S6, pp. S-34 and S-60, respectively). The uncertainty in the tuff data for large driving-stress ratios is accounted for by a linear fit which clearly overestimates the time-dependent degradation observed in the ESF and the ECRB Cross-Drift.

1.3.4 Case Histories of Tunnel Performance

Unsupported or lightly supported tunnels (although perhaps not considered safe from a personnel standpoint) can stand in a stable condition for long time periods, particularly in good quality rock masses. For example, the ESF (approximately 8-km long with a 7.62-m diameter) and ECRB Cross-Drift (approximately 2.5-km long with a 5-m diameter) tunnels at the Yucca Mountain site were constructed in 1995 to 1997 and in 1998, respectively. The ESF main loop is located largely in the middle nonlithophysal stratum (Tptpmn), while the ECRB Cross-Drift cuts through and exposes all of the repository host horizon units. The tunnels are, in general, lightly supported with friction rock bolts and light wire mesh in the tunnel roof, with occasional friction bolts in the tunnel walls. There is no notable evidence of deterioration or degradation of the rock mass, and no significant episodes of rockfall have occurred (BSC 2004, Section 6.4.2.4.1.3, p. 6-193). Note that the ground support is for worker safety and does not prevent degradation of the rock mass from static fatigue.

Hoover Dam, with abutments excavated in Tertiary pyroclastic flows (which are analogous to Yucca Mountain), was completed by the Bureau of Reclamation in 1936 (BSC 2004, Section 6.4.2.4.1.3). Along with the construction of the dam itself are a series of tunnels and adits that were excavated to accommodate the various penstocks, valves, access ways, spillways, and river bypasses. With the exception of the visitor center elevator shaft (completed in the 1990s), the excavations were completed with simple drill and blast methods ("simple" meaning here that no smooth-wall blasting techniques were used). Some of the larger openings, generally those more than 6-m (20-ft) high, were excavated using heading-and-bench methods to develop the full size of the openings. Many of the tunnels and adits were excavated to greater than 12 m (40 ft) in diameter. While some of the penstock and spillway tunnels were lined with concrete, many of the adits and access ways remain unlined.

The rock at the site is the tuff of Hoover Dam, a fairly localized unit composed of andesitic to dacitic pyroclastic flows and breccias. At the dam, the volcanics are slightly to densely welded, and slightly weathered to unweathered. At the penstock adits, the rock is moderately hard to hard and contains abundant lithic fragments and occasional corroded pumice fragments. The rock is slightly to moderately fractured, with most fractures devoid of fracture filling. Many of the discontinuities exposed in the adits are frequently shears and small faults displaying distinct slickensides. Where the adits extend below the phreatic surface, occasional calcium carbonate precipitate is present adjacent to active or old seeps.

The adits were excavated downstream of the power plant to allow insertion of large, steel penstock sections into tunnels that paralleled the canyon walls. The adits are still in use, housing the sewage treatment system and other support utilities necessary to the function of the dam. The adits are approximately 40-ft (12-m) high by 35-ft (10.7-m) wide (BSC 2004, Section 6.4.2.4.1.3, p. 6-195) becoming slightly taller with depth. After the drill and blast excavation, the adits were left unlined and unsupported, and continue to be unsupported to the present time. Rockfall in the adits has been limited to very occasional centimeter-size fragments, even without ground support, over a period of more than 70 years.

Additionally, there are numerous access ways throughout the lower canyon walls in and around the Hoover Dam power plant. These smaller tunnels, 6 to 15 ft (1.8 to 4.6 m) in diameter (BSC 2004, Section 6.4.2.4.1.3, p. 6-195), allow access by personnel and tourists to various areas of the power plant and penstocks. Few of these tunnels are supported either by rock bolts or wire mesh. No steel supports are visible in the Hoover Dam excavations. As with the adits, rockfall in the access ways and tunnels during a period of more than 70 years has been limited to rare centimeter-size fragments that are removed by the janitorial staff.

1.3.5 Impact of Uncertainties on Screening Argument for FEP 2.1.07.02.0A

Because long-term strength predictions (BSC 2004, Section 6.4.2.4 and Appendix S) are based on limited static-fatigue test data, a linear-fit approach that provides a conservative representation for the time-dependent strength degradation of tuff has been used to predict long-term drift degradation. This approach is described in Sections 1.2 and 1.3.1 of this RAI response. The time-dependent strength behavior of tuff is predicted to cause only partial collapse of the drift during the first 10,000 years after repository closure (BSC 2004, Section 8.1, p. 8-3). Subsequent analyses considering a range of thermal loadings have estimated that the increased rockfall volume attributable to time-dependent degradation would amount to approximately 2 m^3/m (SNL 2008a, Section 6.4.1.6, p. 6-89), and have shown that the temperature-limit requirements for the waste packages and the drift wall will be met (SNL 2008a, Table 6.5-4 and Section 7.1). Also, under this condition, the collapse of the drip shield framework is not predicted because vertical loads on the crown of the drip shield will not be significant (SNL 2007, Figure 6-75). The accumulated rockfall volume during 10,000 years is expected to have no significant impact on the thermal requirements of the EBS components and the structural integrity of the drip shield. Furthermore, seepage analyses based on partial drift collapse showed no impacts to seepage (SNL 2008b, FEP 2.1.07.02.0A). Therefore, the uncertainties in time-to-failure of rock will not have a significant effect on long-term repository performance or on the screening arguments that support the exclusion of FEP 2.1.07.02.0A (SNL 2008b, FEP 2.1.07.02.0A).

2. COMMITMENTS TO NRC

None.

3. DESCRIPTION OF PROPOSED LA CHANGE

None.

4. REFERENCES

BSC (Bechtel SAIC Company) 2004. *Drift Degradation Analysis.* ANL-EBS-MD-000027 REV 03. Las Vegas, Nevada: Bechtel SAIC Company. ACC: DOC.20040915.0010; DOC.20050419.0001; DOC.20051130.0002; DOC.20060731.0005; LLR.20080311.0066.

Lama, R.D. and Vutukuri, V.S. 1978. *Handbook on Mechanical Properties of Rocks.* Clausthal, Germany: Trans Tech Publishers. TIC: 209882.

Martin, C.D. 1997. "Seventeenth Canadian Geotechnical Colloquium: The Effect of Cohesion Loss and Stress Path on Brittle Rock Strength." *Canadian Geotechnical Journal, 34,* (5), 698-725. Ottawa, Ontario, Canada: NRC Research Press. TIC: 260303.

Martin, R.J.; Noel, J.S.; Boyd, P.J.; and Price, R.H. 1997. "Creep and Static Fatigue of Welded Tuff from Yucca Mountain, Nevada." *International Journal of Rock Mechanics and Mining Sciences, 34* (3/4), 382. New York, New York: Elsevier. TIC: 250241.

Schmidtke, R.H. and Lajtai, E.Z. 1985. "The Long-Term Strength of Lac du Bonnet Granite." *International Journal of Rock Mechanics and Mining Science & Geomechanics Abstracts, 22* (6), 461-465. New York, New York: Pergamon. TIC: 254874.

Scholz, C.H. 1972. "Static Fatigue of Quartz." *Journal of Geophysical Research, 77* (11), 2104–2114. Washington, D.C.: American Geophysical Union. TIC: 224772.

SNL (Sandia National Laboratories) 2007. *Seismic Consequence Abstraction.* MDL-WIS-PA-000003 REV 03. Las Vegas, Nevada: Sandia National Laboratories. ACC: DOC.20070928.0011; LLR.20080414.0012.

SNL 2008a. *Postclosure Analysis of the Range of Design Thermal Loadings.* ANL-NBS-HS-000057 REV 00. Las Vegas, Nevada: Sandia National Laboratories. ACC: DOC.20080121.0002; LLR.20080408.0251; DOC.20080828.0006.

SNL 2008b. *Features, Events, and Processes for the Total System Performance Assessment: Analyses*. ANL-WIS-MD-000027 REV 00. Las Vegas, Nevada: Sandia National Laboratories. ACC: DOC.20080307.0003; DOC.20080407.0009; DOC.20080722.0002.

RAI: Volume 3, Chapter 2.2.1.2.1, Number 3

Provide a technical basis to support the conclusion that the analysis in Sandia National Laboratories (2008b) indicates stable drift openings whereas the analysis also shows the boundaries of the opening are subjected to stresses greater than the unconfined compressive strength of the surrounding rock. This information is needed to verify compliance with 10 CFR 63.114 (e), (f), (g).

1. RESPONSE

1.1 OVERVIEW

RAI 3.2.2.1.2.1-003 questions whether stable drift openings can exist when the stress at the boundary of an excavation exceeds the unconfined compressive strength. This section provides an overview of the different computational techniques that are used to predict drift degradation and drift stability. The next section, Section 1.2, provides detailed analyses of the response of host rock surrounding a tunnel when the stress at the tunnel wall exceeds the unconfined compressive strength.

The results of the drift stability analysis for extreme thermal loading conditions are reported in *Postclosure Analysis of the Range of Design Thermal Loadings* (SNL 2008), also referred to herein as the thermal loadings report. Those calculations, depending on the loading conditions and the lithophysal rock mass quality, indicate fracturing of the rock mass and different extent of instability and rubble accumulation. In all cases analyzed, the drifts reached stable configurations, shown together with stress tensor plots colored by the magnitudes of the major and minor principal stresses in Figures 6.4.1-4 through 6.4.1-9 of the thermal loadings report (SNL 2008). When fracturing of the rock mass did not result in rockfall, the yielded rock mass was destressed and high stress concentrations were “pushed” away from the boundary where the rock was able to sustain those stresses under confined conditions (e.g., stresses in the drift wall shown in SNL 2008, Figure 6.4.1-4). Thus, the stresses greater than the unconfined compressive strength are not exactly at the boundary of the excavation, but at some distance from the boundary where the rock is stronger due to confinement. If the yielding of the rock results in the rockfall, a breakout is formed, which typically, as in the example shown in Figure 6.4.1-5 of the thermal loadings report (SNL 2008), reaches a stable configuration. Stress state at the tip of the breakout is three-axial, because of relatively small radius of curvature, with large confining stresses allowing also large stress concentrations. The large stress concentrations near the tip of the breakout can be seen in drift crown in Figure 6.4.1-5a of the thermal loadings report (SNL 2008). However, Figure 6.4.1-5b of that report (SNL 2008) illustrates large confining stresses extending to the tip of the breakout, making rock stronger and capable to sustain those large stress concentrations. Enlarged stress tensor plots from Figures 6.4.1-5a and 6.4.1-5b of the thermal loadings report (SNL 2008) at 95 years for the lithophysal rock mass Category 3 (with unconfined compressive strength of 20 MPa; BSC 2004, Table 6-41), illustrating the stress concentrations due to tri-axial stress state near the corners, are shown in Figure 1-1.

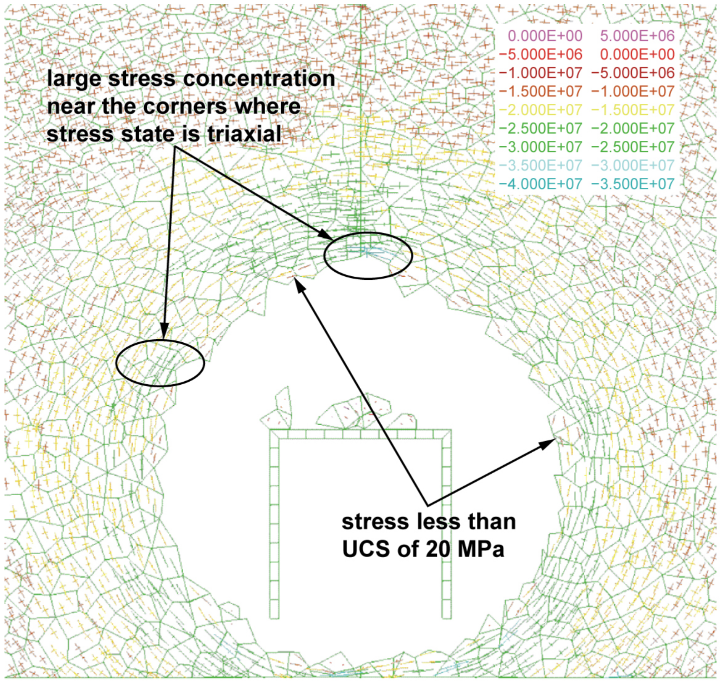

a) Major Principal Stress (Pa)

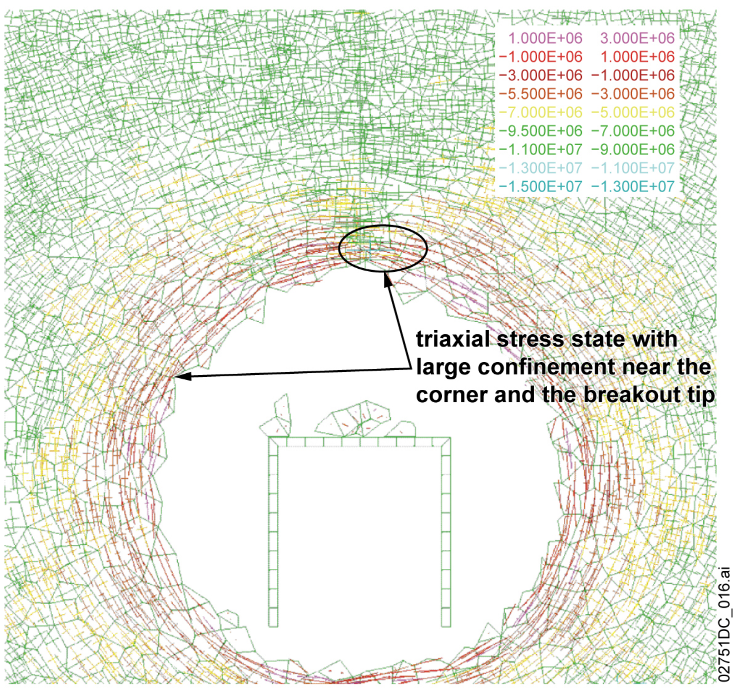

b) Minor Principal Stress (Pa)

Source: DTN: MO0707THERMRES.000, folder: \Scenario 1\category 3, files: *case2jointing3age95sig1.pcx* and *case2jointing3age95sig2.pcx*.

Figure 1-1. Drift Configuration and Stresses for Case 1 Extreme Thermal Loading (SNL 2008, Section 6.4.1.5) at 95 years, Category 3 Lithophysal Rock Mass

In the NRC's Background section for RAIs 3.2.2.1.2.1-001 through 3.2.2.1.2.1-006, the NRC also states that "a DOE analysis for the combined effects of rock weakening and thermal loading of a drift in Category 5 lithophysal rock mass does not show significant drift degradation at 80 years (Bechtel SAIC Company, 2004, Figure S-44), although DOE data (Bechtel SAIC Company, 2004, Figure S-29) and analysis (Bechtel SAIC Company, 2004, Section 6.4.2.3.1) indicate the prevailing stresses should result in roof failure in less than 32 years." This statement implies that if the elastically calculated stresses exceed the unconfined compressive strength of the rock (accounting for time-dependent weakening), the drifts should collapse. However, standard rock mechanics textbooks support the stability of underground openings when the rock at the wall of the excavation has yielded (see quotes in Section 1.2).

Stability of the emplacement drifts in the lithophysal rock was analyzed using three different conceptual models. The results of the analyses are documented in detail in *Drift Degradation Analysis* (BSC 2004). A discontinuum approach based on Voronoi blocks was the main method for the stability analysis. The results of the discontinuum analyses were also corroborated by the results from various continuum approaches (BSC 2004, Section 7.6.5.4) based on elastic and elasto-plastic constitutive models. The results from the different conceptual models are in agreement with each other and are generally consistent with field observations. For example, elastic analyses show that, during the thermal pulse (between closure of the repository and approximately 3,000 years), the thermally induced elastic stresses exceed the strength of the lithophysal rock for rock mass Categories 2, 3, 4, and 5 in a narrow ring of rock in the drift crown (e.g., BSC 2004, Figure 6-144). The maximum depth of the "overstressed" rock is 0.17 m for Category 5 lithophysal rock mass. Similarly, the elastic stresses in the drift wall (~17.5 MPa) under in situ conditions are greater than the strength of lithophysal rock mass for rock mass Categories 1 and 2 (e.g., BSC 2004, Figure 6-141).

All models with a post-yielding material behavior that is consistent with laboratory testing predict a stable drift configuration throughout the thermal cycle, with minor, inconsequential rockfall. The discontinuum model exhibits fracturing in the "overstressed" region and minor rockfall. The elasto-plastic model results in yielding in the regions of elastically predicted "overstressed" rock. ("Overstressed" rock refers to rock that has exceeded its yield strength, but is not allowed to yield in an elastic model.) Only the elasto-plastic model with the extremely unrealistic assumption of infinitely brittle softening and no residual cohesion (fourth row in Figure 7-43 of BSC 2004) predicts a progressive drift collapse.

1.2 YIELDING OF ROCK AND STABILITY OF TUNNELS

Yielding of rock at an excavation wall does not necessarily result in rockfall or in an unstable underground opening. When the elastic stress on the tunnel boundary exceeds the unconfined compressive strength of the surrounding rock, the rock yields or fails plastically. The underlying mechanisms that result in yielding of hard rocks are fracturing (initiation of new or propagation of existing fractures) and/or slip on pre-existing joints.

The following three quotes from standard rock mechanics textbooks support the stability of underground openings when the rock at the wall of the excavation has yielded:

- In *Support of Underground Excavations in Hard Rock*, Hoek et al. (2000, Section 9.2.3) state:

> Note that plastic failure of the rock mass surrounding the tunnel does not necessarily mean that the tunnel collapses. The failed material still has considerable strength and, provided that the thickness of the plastic zone is small compared with tunnel radius, the only evidence of failure may be a few fresh cracks and a minor amount of raveling or spalling. On the other hand, when a large plastic zone is formed and when large inward displacements of the tunnel wall occur, the loosening of the failed rock mass will lead to severe spalling and raveling and to an eventual collapse of an unsupported tunnel.

- In *Rock Mechanics for Underground Mining*, Brady and Brown (1985, Section 7.5) note that:

> In assessing the performance of excavations and rock structures, it is useful to distinguish between failure of the structure, and failure or fracture of the rock mass. Failure of a structure implies that it is unable to fulfill the designed duty requirement. Failure of a rock structure in massive rock is synonymous with extensive rock fracture, since the stable performance of the structure under these conditions cannot be assured. In a mine structure, control of displacements in a fractured rock mass may require the installation of design support elements, or implementation of a mining sequence which limits the adverse consequences of an extensive fracture domain. On the other hand, limited fractured rock zones may pose no mining problem, and a structure or opening may completely satisfy the design duty requirements.

- In *Fundamentals of Rock Mechanics,* Jaeger and Cook (1979, Section 18.2) state:

> However, in many excavations, especially those resulting from mining, it is not possible to keep the stresses everywhere in the rock less than its strength. Neither does experience indicate that this is necessary to ensure the stability of the excavation. The rock fails in parts surrounding many underground excavations, but only occasionally does this impair the stability or safety of excavations. The criterion that the stresses must always be less than the strength may therefore be sufficient to ensure the stability of a structure, but it is certainly not necessary. … Observation of underground excavations surrounded by failed rock often shows that this rock, though failed, is still subject to stress. … while the stresses in the failed rock must have exceeded its strength, the stresses applied to it are in stable equilibrium with its resistance to them.

Another illustration of the effect of "overstressed," or yielded, rock is the observed behavior of the tunnels in the Exploratory Studies Facility (ESF) main loop and in the Enhanced Characterization of the Repository Block (ECRB) Cross-Drift. The in situ stresses at depths between 300 m and 350 m are approximately 7 MPa in the vertical direction and 3.5 MPa in the horizontal direction (BSC 2004, Figure 6-139). Using the classical formula for elastic stress concentration (e.g., Goodman 1980, Section 7.2), the maximum stress in the drift wall is estimated to be:

$$\sigma_{\max} = 3\sigma_1 - \sigma_3 = 3 \times 7 - 3.5 = 17.5\,\text{MPa}$$

This elastic stress concentration exceeds the strength of lithophysal rock mass Categories 1 and 2, which have unconfined compressive strengths of 10 MPa and 15 MPa (BSC 2004, Table E-10), respectively. The "overstressed" conditions are confirmed by observation of fractures that are parallel and close to the drift wall, based on a horizontal borehole drilled in the springline of the ESF, south ramp, excavated in the lowest-quality lithophysal rock (BSC 2004, Figure 7-2). Although the ESF and the ECRB are only supported in the crown by rock bolts and wire mesh (i.e., no support in the drift walls), the drifts have been stable for more than 10 years. The rock yielded (as evidenced by fractures), but the excavation does not fail. This observation is consistent with the quotes on the previous page. The yielding of rock around the emplacement drifts under thermally induced stresses will occur predominantly in the drift crown, but will be manifested in a similar manner.

Figure 1-2 illustrates the concept of yielding and stress redistribution in the rock surrounding a tunnel. It shows the region of plastic deformation (left) and contours of the major principal stress (right) for an elasto-plastic, cohesion softening material. In this example, the far-field stress state causes rock to yield near the drift wall and to transfer stress further into the rock mass, similar to the expected behavior for the poorest quality lithophysal rock mass.

This failed rock near the drift wall is sometimes referred to as "overstressed" because an elastic model can predict stresses that exceed the yield strength. However, "overstress" does not exist in reality or in realistic constitutive models. It is a concept used to estimate the extent of yielding based on elastically calculated stresses—i.e., to determine the regions where the elastically calculated stress exceeds the rock strength. In reality, when the rock is strained beyond the level that corresponds to its yield strength, two processes take place. The rock strength starts to decrease (assuming softening post-yield response), and the yielded rock undergoes additional deformation as it becomes "softer." That additional deformation results in stress redistribution, in which the stress concentration moves from the yielded region to a region farther away from the surface of the excavation, where confining stresses and, consequently, the strength are greater (as illustrated by the stress contours in Figure 1-2).

The entire process and its effect on stability of the excavation is discussed by Jaeger and Cook (1979, Section 18.2). If the material response is not very brittle, the yielded zone will destress below its post-peak strength, with more of the load being transferred to the (confined) elastic region. In this way, the excavation reaches a stable equilibrium with no instability. In the example shown in Figure 1-2, equilibrium is reached, and the yielded zone, which has softened, still carries significantly reduced, but finite, stresses.

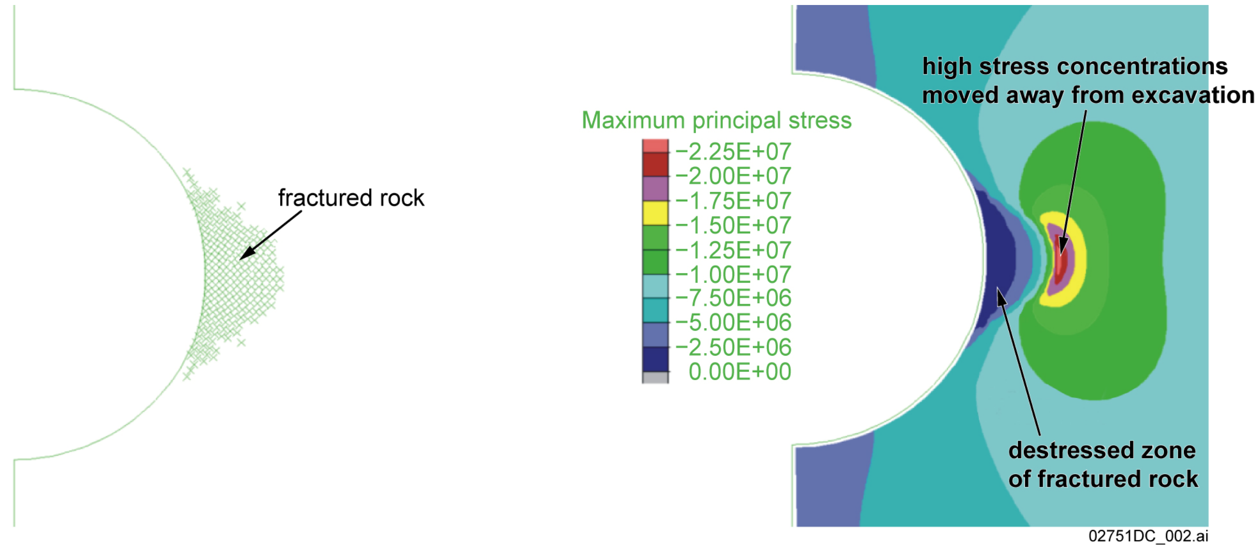

Source: For illustrative purposes only.

Figure 1-2. Yielded Zone and Contours of Major Principal Stress (Pa) around a Circular Tunnel

In the case of a very brittle material response, the stress reduction occurs at a slower rate (with respect to strain) than strength softening. In this situation, those portions of the tunnel periphery will be unstable where the cohesive strength has dropped to zero, resulting in breakout from the tunnel walls. Empirical evidence (Kaiser et al. 2000, Figure 3.12) shows that the depth of breakout in massive, brittle rock can be related to the ratio between the maximum tangential stress, $\sigma_{\max}$, and the intact (laboratory) rock strength, σ_c. This empirical experience also shows that, for brittle rocks where yielding results in instability, the breakouts reach finite depth and tunnels eventually achieve a long-term stable unsupported configuration for a wide range of $\sigma_{\max} / \sigma_c$ ratios.

Two examples of idealized stress-strain curves for rocks are shown in Figure 1-3. The typical curve, shown on the left, has some finite ductility (i.e., it softens over a finite strain to a non-zero residual strength). The extreme case of perfectly brittle material response is shown on the right in Figure 1-3. As soon as a perfectly brittle material yields, it completely loses its strength and fails. Only in the case of the perfectly brittle material response is yielding of the material a sufficient condition for tunnel instability.

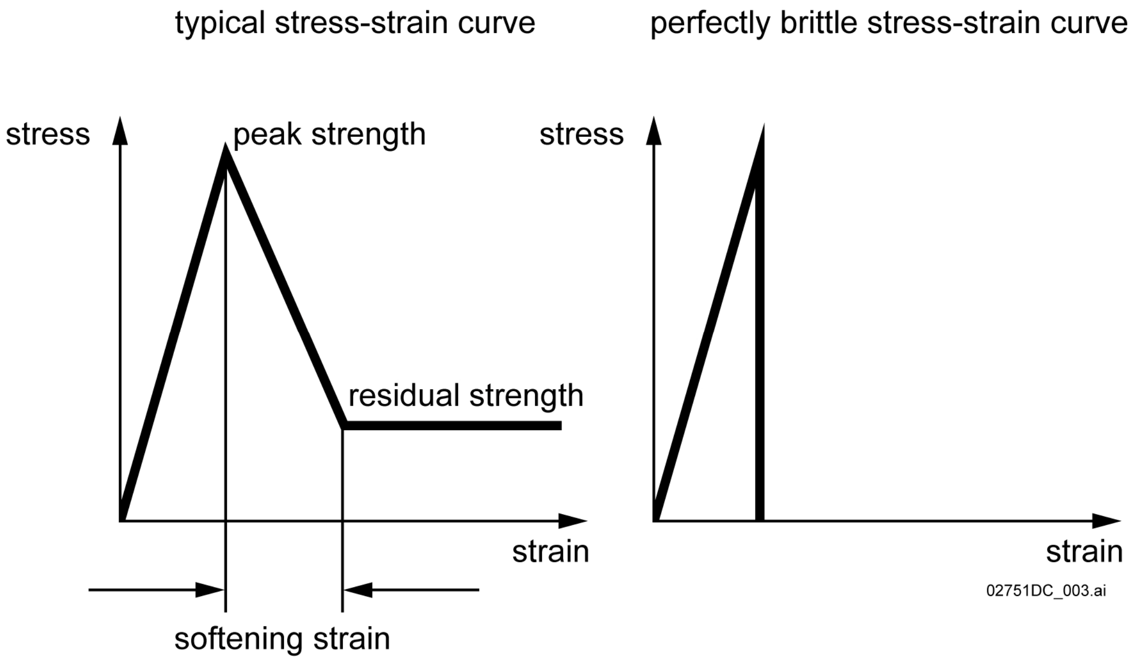

Source: For illustration purposes only.

Figure 1-3. Examples of Idealized Stress-Strain Curves for Rocks

The continuum elasto-plastic and discontinuum Voronoi block models that have been used to assess emplacement drift stability in Drift Degradation Analysis (BSC 2004) generally include some finite post-peak material ductility and strength (as shown on the left in Figure 1-3). (The exception is one elasto-plastic case with a perfectly brittle response.) However, the computational models are purposely developed to exhibit more brittle behavior than the tuff response observed from laboratory testing. This was done to provide conservatism in the estimate of potential progressive collapse of the drifts. Figure 1-4, for example, shows a comparison of the stress-strain curves for Category 4 lithophysal rock mass obtained for the Voronoi block model and the curve observed in the laboratory. It is seen that the Voronoi model exhibits a more brittle model response. Thus, both the continuum elasto-plastic models (BSC 2004, Section 7.6.5.4) and Voronoi block models overestimate material brittleness and conservatively represent rock strength softening and stress redistribution as the rock yields. Consequently, the models provide a realistic but bounding prediction of drift stability as the the rock yields.

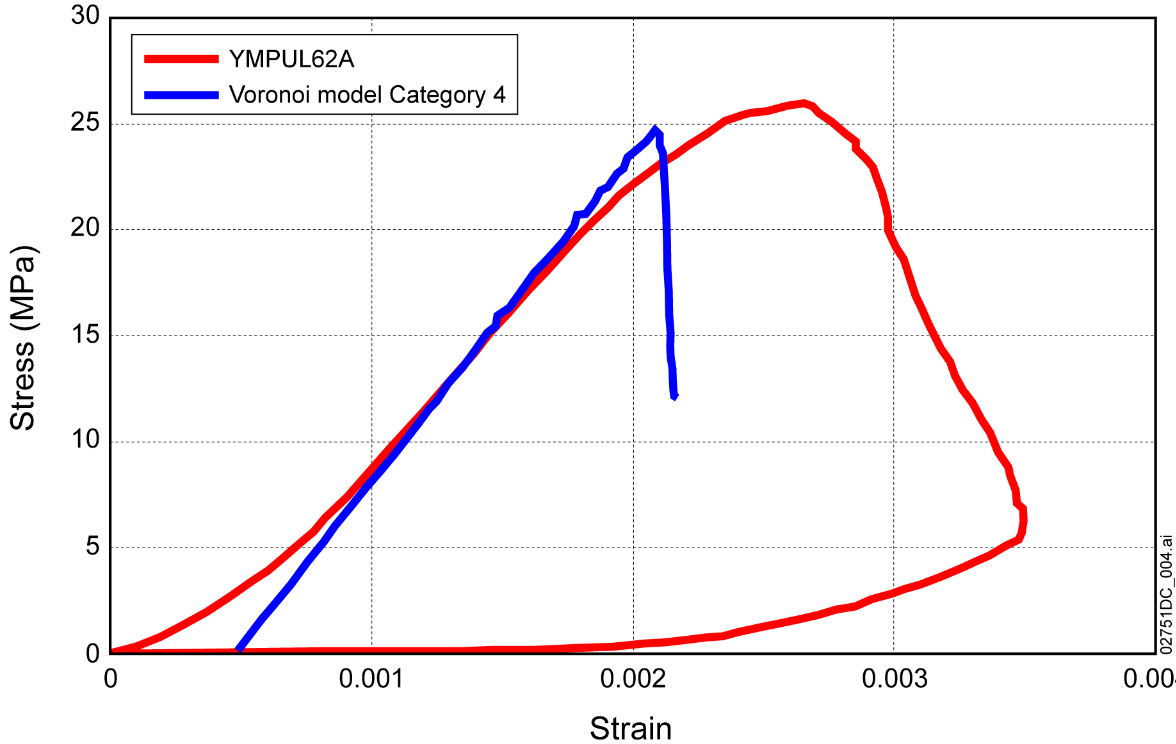

Source: Voronoi block model results from DTN: MO0408MWDDDMIO.002; test data for YMPUL62A, supporting data for DTN: SN0208L0207502.001 in ACC: MOL.20021121.0067, file: *Bs 1 2 SS.xls.*

Figure 1-4. Comparison of Stress-Strain Curves Measured in the Laboratory on a Lithophysal Sample and Obtained by Voronoi Block Model Calibration

2. COMMITMENTS TO NRC

None.

3. DESCRIPTION OF PROPOSED LA CHANGE

None.

4. REFERENCES

Brady, B.H.G. and Brown, E.T. 1985. *Rock Mechanics for Underground Mining*. London, United Kingdom: George Allen and Unwin. TIC: 226226.

BSC (Bechtel SAIC Company) 2004. *Drift Degradation Analysis*. ANL-EBS-MD-000027 REV 03. Las Vegas, Nevada: Bechtel SAIC Company. ACC: DOC.20040915.0010; DOC.20050419.0001; DOC.20051130.0002; DOC.20060731.0005; LLR.20080311.0066.

Goodman, R.E. 1980. *Introduction to Rock Mechanics.* New York, New York: John Wiley & Sons. TIC: 218828.

Hoek, E.; Kaiser, P.K.; and Bawden, W.F. 2000. *Support of Underground Excavations in Hard Rock*. Rotterdam, The Netherlands: A.A. Balkema. TIC: 252991.

Jaeger, J.C. and Cook, N.G.W. 1979. *Fundamentals of Rock Mechanics.* 3rd Edition. New York, New York: Chapman and Hall. TIC: 218325.

Kaiser, P.K.; Diederichs, M.S.; Martin, D.; Sharpe, J. and Steiner, W. 2000. "Invited Keynote: Underground Works in Hard Rock Tunnelling and Mining." *GeoEng2000 International Conference on Geotechnical & Geological Engineering.* Lancaster, PA: Technomic. TIC: 254732.

MO0408MWDDDMIO.002. Drift Degradation Model Inputs and Outputs. Submittal date: 11/26/2008.

SN0208L0207502.001. Mechanical Properties of Lithophysal Tuff, Batch #1 (Test Dates: July 31, 2002 through August 16, 2002). Submittal date: 08/20/2002.

SNL (Sandia National Laboratories) 2008. *Postclosure Analysis of the Range of Design Thermal Loadings*. ANL-NBS-HS-000057 REV 00. Las Vegas, Nevada: Sandia National Laboratories. ACC: DOC.20080121.0002; LLR.20080408.0251; DOC.20080828.0006.

RAI: Volume 3, Chapter 2.2.1.2.1, Number 4

Explain the calculated damage pattern depicted in Figure S-32 of Bechtel SAIC Company (2004), which shows more rock damage inside the rock mass at a distance from the opening than at the boundary of the opening. The explanation should identify the natural process included in the model that would cause more rock damage inside the rock mass than at the boundary of the modeled underground opening. This information is needed to verify compliance with 10 CFR 63.114 (e), (f), (g).

1. RESPONSE

The conceptual model and calculations for the effect of time-dependent strength degradation on drift stability in lithophysal rock is documented in Section 6.4.2.4 and in Appendix S of *Drift Degradation Analysis* (BSC 2004). Details of the conceptual model for time-dependent strength degradation are presented in Section S3.3 of that report (BSC 2004).

Strength degradation in the lithophysal rock mass is represented by reducing the cohesive strength of the contacts between Voronoi blocks as a function of driving stress (i.e., the stress state) and time. The contacts gradually accumulate damage with time in accordance with a static-fatigue curve fitted to experimental data. Cohesion and tensile strength of a contact at a given time are proportional to its initial strength and accumulated damage, which varies between 0 (no damage) and 1 (complete damage—i.e., no strength). Once a contact fails, either in shear or tension, a fracture develops between the blocks, and the fracture behaves as a simple frictional contact that has permanently lost all cohesion and tensile strength. Figure S-32 in *Drift Degradation Analysis* (BSC 2004) shows a typical example for the state of the lithophysal rock at 500 years after excavation of the drift. The properties in the example are based on lithophysal rock mass Category 2 and the best-fit static fatigue curve for lithophysal rock. This figure is reproduced here with some additional annotation as Figure 1-1. The explanation of the plots included in Figure 1-1 is provided in the note to the figure.

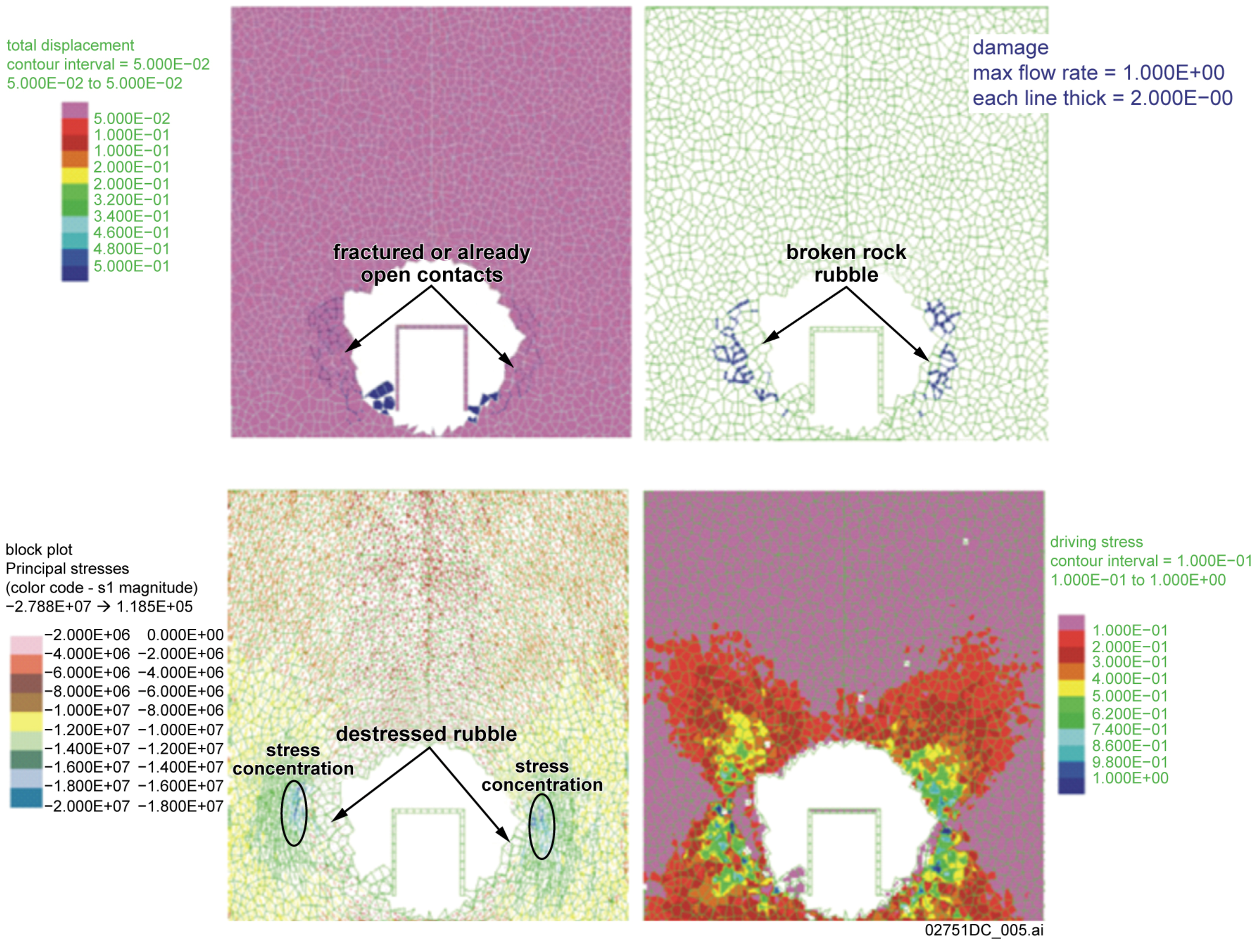

Source: BSC 2004, Figure S-32, with additional notes.

NOTE: The top left figure shows the contours of displacement magnitudes (m) and fractures in the rock mass (blue lines); the top right figure shows accumulated damage, where the thickness of a blue line is proportional to the accumulated damage (between 0 and 1); the bottom left figure shows the principal stress tensors (Pa) colored by the magnitude of the major principal stress; the bottom right figure shows the contours of the scaled driving stress (between 0 and 1).

Figure 1-1. Model State for Rock Mass Category 2 Lithophysal Rock after 500 Years

The top right plot in Figure 1-1 illustrates the damage accumulated in those contacts which are not fractured and broken (i.e., have undergone certain relative displacement). Once a contact is fractured, the accumulated damage is irrelevant and is therefore discarded; hence, it does not show up in the top right plot. The top right plot shows that there are damaged contacts within the rock mass, but apparently no damaged contacts at the surface of the excavation. In fact, the rock directly adjacent to the tunnel is already completely fractured and broken. This can be confirmed in the fracture plot (the top left plot), in the stress tensor plot (the bottom left plot), and in the contour plot of the scaled driving-stress ratio (the bottom right plot). The fracture plot indicates that the region directly adjacent to the tunnel is already fractured, based on the presence of blue lines along the fractured contacts. The stress tensor and the driving-stress ratio plots show that the fractured region adjacent to the tunnel is almost completely distressed, consistent with the fact that the rock is severely broken. The output data (DTN: MO0408MWDDDMIO.002) from *Drift Degradation Analysis* (BSC 2004) provide additional details for the damage around the boundary of the opening as shown in Figures 1-2 and 1-3. The detail of damage plot on larger scale is shown in Figure 1-2, in which opening of some of the joints in the broken rock mass is apparent. This interpretation also is confirmed by Figure 1-3, which shows the state of the same simulation at 10 years after excavation. Figure 1-3 confirms that the rock directly adjacent to the excavation is already damaged after 10 years.

Thus, the damage pattern depicted in Figure S-32 of *Drift Degradation Analysis* (BSC 2004), which shows more rock damage inside the rock mass at a distance from the opening than at the boundary of the opening, is a consequence of large displacements of already fractured rock mass near the boundary of the opening, which is a natural process included in the model; it is not an incorrect representation of the mechanical process.

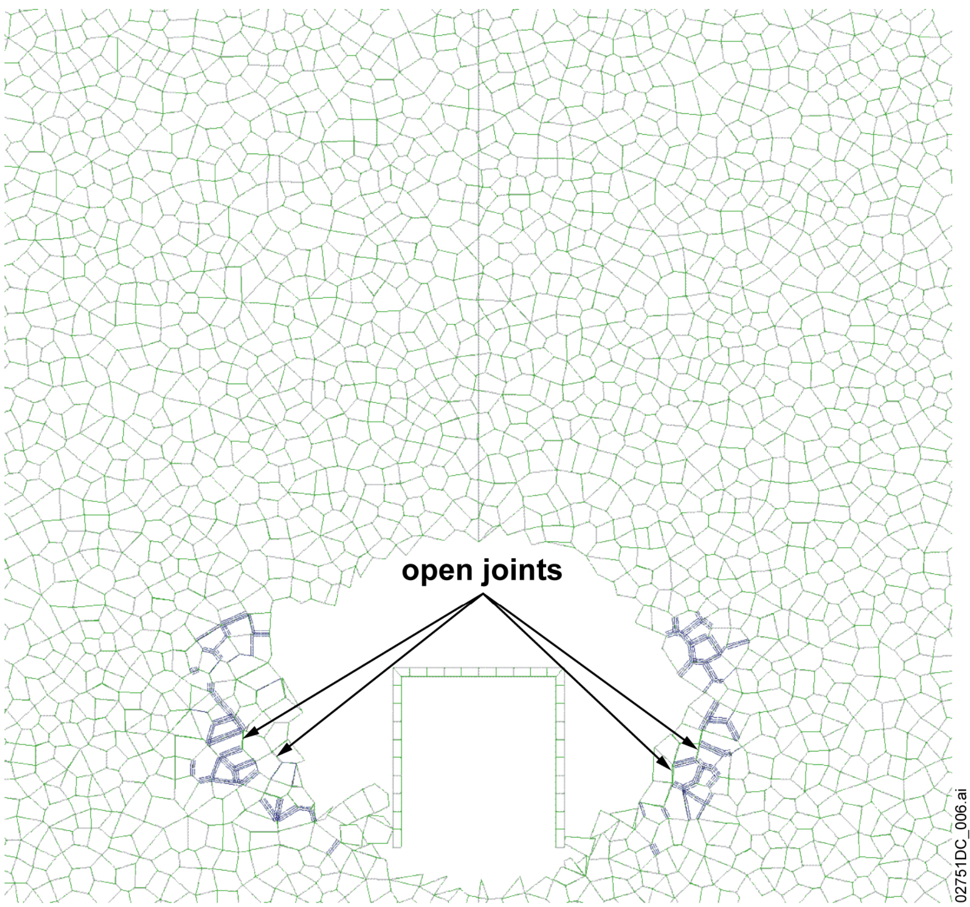

Source: DTN: MO0408MWDDDMIO.002, compressed file: *2.1c_UDEC Lithophysal Inputs and Outputs.zip*, folder: \lithophysal\time-dependent\degradation\Category 2 tuff best fit, file: *Case12property2age500_damage.bmp*.

NOTE: The figure shows accumulated damage, where the thickness of the blue lines are proportional to the accumulated damage (between 0 and 1).

Figure 1-2. Detail of Damage in Rock Mass Category 2 Lithophysal Rock after 500 Years

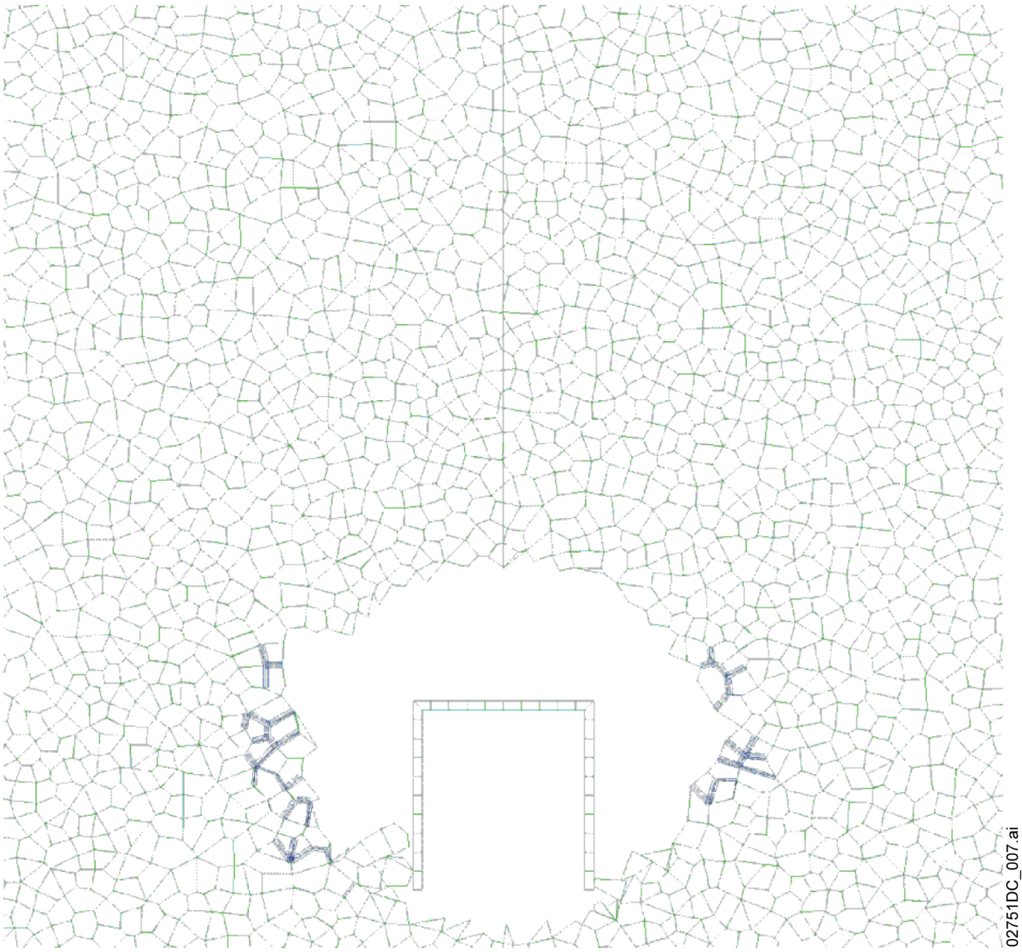

Source: DTN: MO0408MWDDDMIO.002, compressed file: *2.1c_UDEC Lithophysal Inputs and Outputs.zip*, folder: \lithophysal\time-dependent\degradation\Category 2 tuff best fit, file: *Case12property2age10_damage.bmp*.

NOTE: The figure shows accumulated damage, where the thickness of the blue lines are proportional to the accumulated damage (between 0 and 1).

Figure 1-3. Detail of Damage in Rock Mass Category 2 Lithophysal Rock after 10 Years

2. COMMITMENTS TO NRC

None.

3. DESCRIPTION OF PROPOSED LA CHANGE

None.

4. REFERENCES

BSC (Bechtel SAIC Company) 2004. *Drift Degradation Analysis*. ANL-EBS-MD-000027 REV 03. Las Vegas, Nevada: Bechtel SAIC Company. ACC: DOC.20040915.0010; DOC.20050419.0001; DOC.20051130.0002; DOC.20060731.0005; LLR.20080311.0066.

MO0408MWDDDMIO.002. Drift Degradation Model Inputs and Outputs. Submittal date: 11/26/2008.

RAI Volume 3, Chapter 2.2.1.2.1, Number 5

Provide a technical basis for the calibration of the inelastic behavior of the rock mass in the model, or demonstrate that the model is insensitive to this inelastic behavior. This information is needed to verify compliance with 10 CFR 63.114 (e), (f), (g).

1. RESPONSE

1.1 TECHNICAL BASIS FOR CALIBRATION OF ELASTIC AND INELASTIC BEHAVIOR

This section provides the technical basis for calibration of elastic (Young's modulus) and inelastic (unconfined compressive strength) behavior of rock mass in the model. The Voronoi block model used in the analyses of long-term drift stability (including the effects of thermally induced stresses and time-dependent strength degradation), reported in *Drift Degradation Analysis* (BSC 2004), was calibrated to the results of unconfined compressive tests carried out on large-core samples of the lithophysal rock mass. The axial load and axial and lateral strains were measured during the laboratory tests. The tests were carried out at least until the peak axial stress was reached; in some cases, the deformation went far beyond the peak stress. In all cases, a portion of the post-peak stress-strain response was measured and clearly indicated a finite ductility in the sample response (i.e., no sample failed violently) before the sample was unloaded. The measured data were used to calculate elastic constants, specifically Young's modulus and Poisson's ratio, the ultimate strength, and the axial strain at failure (Price 2004, Section 4.0).

The parameters that have the greatest effect on drift stability and that can be measured with greatest reliability in the compression tests are the elastic properties (e.g., Young's modulus and Poisson's ratio) and the uniaxial compressive strength (UCS), which is an inelastic material property. The elastic properties (i.e., the stiffness) of the rock mass control the magnitude of the thermally induced stresses (for the given coefficient of thermal expansion which is independent of rock mass quality). The UCS of the rock mass defines the stress level in the drift wall at which the rock mass yields (but not necessarily when the rock mass fails and produces rockfall). These properties were measured (or calculated directly from the measured data) and the Voronoi block model for the drift stability calculations was calibrated directly to the stiffness and the strength of the lithophysal rock mass. The technical basis for calibration of the stiffness and the UCS of the rock mass is discussed in detail in *Drift Degradation Analysis* (BSC 2004, Section 7.6.4).

1.2 MODEL INSENSITIVITY TO OTHER ASPECTS OF INELASTIC BEHAVIOR

This section provides a discussion that the model is either insensitive to inelastic behavior, or is conservative in its representation of rockfall. The focus of the rest of the response is the other aspects of inelastic behavior to which the model is not directly calibrated as stated in the Background section of the RAI: "The inelastic behavior of the model (e.g., relationship between dilational and shearing strains), however, was not calibrated." It is demonstrated in the following text that the model is either insensitive to this inelastic behavior, or that the model response overpredicts and bounds rockfall and rubble accumulation. Other aspects of inelastic behavior (besides the UCS) that can affect drift stability are:

- Post-peak stress-strain curve of the lithophysal rock mass,
- Rock mass friction angle,
- Irreversible volume change (or dilation) due to yielding of the rock mass, and
- Tensile strength of the rock mass.

Each of these aspects, their effect on drift stability, their representation in the numerical model, and the effects of their representation on prediction of drift stability and rockfall, are discussed separately in the following text.

1.2.1 Post-Peak Stress-Strain Curve

The post-peak stress-strain curve is an important parameter affecting the stability of an underground excavation. In many circumstances (particularly in mining), it is impossible to design underground excavations using the condition that the rock mass deforms only elastically. For example, Jaeger and Cook (1979, Section 18.2, "Criteria for the design and support of underground excavations") state:

> However, in many excavations, especially those resulting from mining, it is not possible to keep the stresses everywhere in the rock less than its strength. Neither does experience indicate that this is necessary to ensure the stability of the excavation. The rock fails in parts surrounding many underground excavations, but only occasionally does this impair the stability or safety of excavations. The criterion that the stresses must always be less than the strength may therefore be sufficient to ensure the stability of a structure, but it is certainly not necessary.

Further, in the same section, the authors state that "… unstable failure cannot occur when the stresses are adequate [i.e., elastically calculated stresses exceed the strength] if insufficient energy is available." For the case of a circular tunnel subject to a hydrostatic field stress, the energy-based concept of tunnel stability can be expressed (Jaeger and Cook 1979, Section 18.2, Equation 1-1) as:

$$\left|\frac{d\sigma}{d\varepsilon}\right| < |k| \qquad \text{(Eq. 1-1)}$$

where σ and ε are the tangential stress and strain in the ring of yielded rock surrounding the tunnel, and k is the stiffness in terms of tangential stress and strain in the surrounding elastic rock. This condition is illustrated graphically in Figure 1-1.

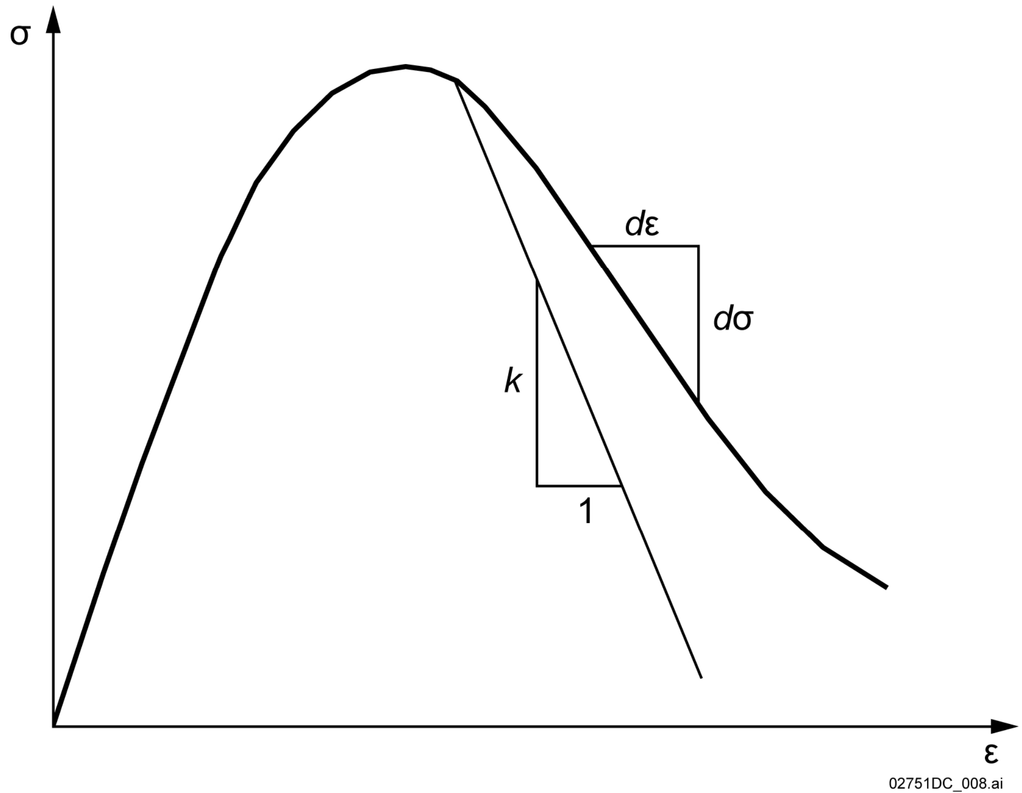

Source: For illustration purposes after Figure 18.2(a) in Jaeger and Cook 1979.

Figure 1-1. Stability Condition as a Function of Softening Slope and Stiffness of the Elastic Rock

Thus, if the elastic stresses exceed the strength of the rock mass, the stability of the yielded rock is a function of the post-peak portion of the stress-strain curve. Rock with more brittle material response (large $d\sigma / d\varepsilon$) will be more prone to rockfall; rock with more ductile material response (small $d\sigma / d\varepsilon$) will result in a more stable underground excavation.

The post-peak softening portion of stress-strain curves for rocks is generally more difficult to measure and is much more random than loading stiffness (i.e., illustrated by scatter in the brittleness index, which is the ratio between the slope of the descending portion of the stress-strain curve and Young's modulus, as measured by Ribacchi 2000, Figure 14). There also is a strong size effect on the post-peak softening response (Bazant and Chen 1997, Section 2, Figure 7). Therefore, instead of calibrating the Voronoi block model to match the average softening stiffness, it was decided to generate the Voronoi block model in such a way that the softening stiffness, $d\sigma / d\varepsilon$, significantly overestimates the stiffness of the lithophysal rock mass. In other words, the Voronoi block model representation of the lithophysal rock mass is more brittle (for unconfined conditions) than the lithophysal rock mass. Thus, the numerical representation is conservative in terms of its likelihood to predict progressive tunnel collapse and rockfall.

The stress-strain curves obtained during calibration of the Voronoi block model for the Category 1 lithophysal rock mass are shown in *Drift Degradation Analysis* (BSC 2004, Figure 7-20). The curve for unconfined compression shows very brittle post-peak response. Figure 1-2 shows a direct comparison of the measured and calibrated curves for the Category 4 lithophysal rock mass. Figure 1-2 demonstrates that the Voronoi model has a very brittle post-peak response in comparison to the experimental data.

The laboratory results on smaller, less fractured samples overestimate brittleness of the rock mass. With increased fracturing, the deformation and yielding of the rock mass occur by deformation and slipping of pre-existing joints, leading to a weaker rock mass with more ductile response. This observation is consistent with the recommendations of Hoek (2007, Chapter "Rock mass properties", Section "Post-failure behavior", Figure 10), who suggests using: 1) an elastic-brittle approximation for a very good quality, hard rock masses, 2) a strain-softening response for an average quality rock masses, and 3) an elastic-perfectly plastic (i.e., ductile) response for very poor quality, soft rock masses.

The Voronoi block model, as shown in *Drift Degradation Analysis* (BSC 2004, Figure 7-20), exhibits increasing ductility with increasing confinement. Such a trend is in qualitative agreement with underground observations and test results (i.e., Ribacchi 2000, Figure 14). However, the brittleness of lithophysal tuff under confined conditions has a second-order effect on drift stability, because yielding first occurs within a relatively narrow region along the drift walls, where the confining stresses are practically zero.

The Voronoi block model clearly shows a more brittle response than that of the actual lithophysal tuff rock mass. Thus, the model will bound and over-predict rockfall.

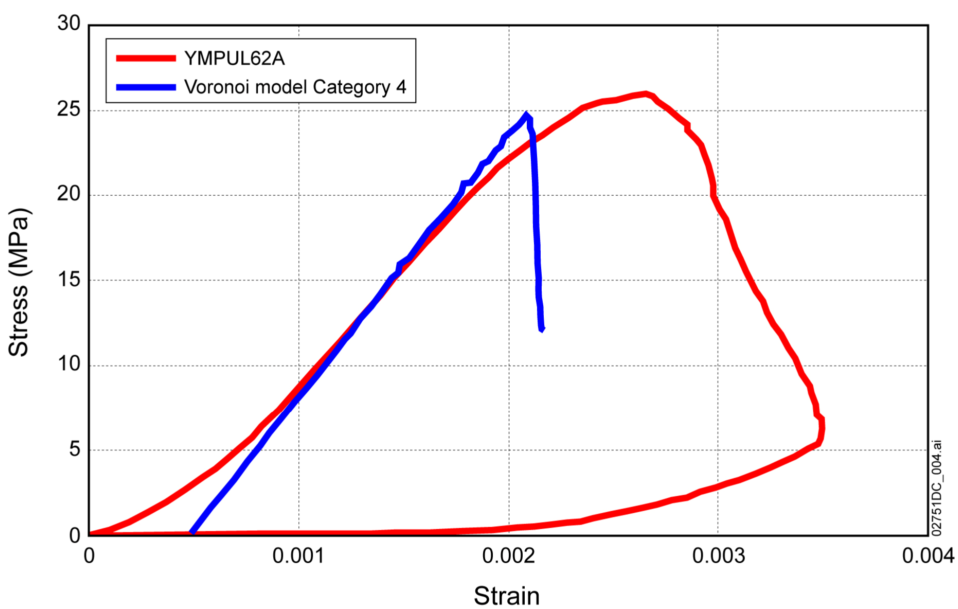

Source: DTN: MO0408MWDDDMIO.002, Voronoi block model results; DTN: SN0208L0207502.001, test data for YMPUL62A, supporting data ACC: MOL.20021121.0067, file: *Bs 1 2 SS.xls*.

Figure 1-2. Comparison of a Stress-Strain Curve Measured in the Laboratory during Unconfined Compression Test on a Large Lithophysal Sample with That Obtained By Voronoi Block Model Calibration

1.2.2 Rock Mass Friction Angle

The rock mass friction angle is an important parameter that characterizes the increase in rock mass strength with increase in confinement. Rock mass friction angles are usually determined through triaxial compression tests with different confining stresses. Confined triaxial testing was not performed on large-diameter, lithophysal rock mass samples because of difficulties in applying confinement to the lithophysal rock. Consequently, the Voronoi block model of the lithophysal rock mass was not calibrated to the specific friction angle. This is not important for this application because yielding first occurs within the relatively thin region along the drift wall. The confining stress in that narrow region is either zero or very small, so yielding occurs in effectively unconfined conditions. The condition for failure of the lithophysal rock mass around the drifts is expressed sufficiently accurately by the UCS, which was measured in the laboratory.

Although the equivalent friction angle of the Voronoi block representation of the lithophysal rock mass was not calibrated directly, its value in the model is set to under-predict the estimated friction angle. The lower friction angle results in a lower strength under confined conditions if the UCS values are the same. For example, the friction angle for the Category 1 lithophysal rock mass (as shown in BSC 2004, Figure 7-21) is 33°. Because of the general non-linearity of the failure surface, the equivalent friction angle is a function of the confining stress, σ_3. To the extent that the friction angle affects drift stability, a friction angle at lower confining stress is of interest. The friction angle of the rock mass can be estimated using the following formula (Hoek 2007, Chapter "Rock mass properties," Section "Mohr-Coulomb parameters," Equation 16):

$$\phi = \sin^{-1}\left[\frac{6am_b(s+m_b\sigma_{3n})^{a-1}}{2(1+a)(2+a)+6am_b(s+m_b\sigma_{3n})^{a-1}}\right] \qquad \text{(Eq. 1-2)}$$

where $\sigma_{3n} = \sigma_{3\max}/\sigma_{ci}$; $\sigma_{3\max}$ is the upper limit of confining stress over which the Hoek-Brown failure criterion is approximated by the Mohr-Coulomb criterion; σ_{ci} is the intact rock strength; and a, m_b and s are Hoek-Brown failure parameters, which are functions of the geological strength index (GSI), and defined in equations E-12 through E-14 of *Drift Degradation Analysis* (BSC 2004). The GSI could not be determined for the lithophysal rock mass because the effect of lithophysal porosity is not taken into account in the classification. However, the GSI for a lithophysal rock mass can be bounded with very high confidence between 20 and 80. (For example, based on Hoek 2007, Table 5 in "Rock mass properties," the GSI 20 is for disintegrated, poor rock; the GSI 80 is for intact or massive, very good rock. The GSI of the lithophysal rock mass is certainly greater than 20 and less than 80; it is probably in the range between 45 and 60.) If the intact rock strength is taken to be 189 MPa (BSC 2004, Table E-14), and the disturbance factor, D (which affects m_b and s), conservatively is assumed to be 1.0, the friction angles of the lithophysal rock (for $\sigma_{3\max} = 1\,\text{MPa}$, to provide an estimate of friction angle at small confinements, which are relevant for drift wall stability) are estimated (using Equation 1-2 and the approach discussed in Section E4.2 of *Drift Degradation Analysis* (BSC 2004) to be 35° and 69° for GSI values of 20 and 80, respectively. (For $D = 0$, which is a better representation of the conditions of drift excavation, the friction angle is estimated to be 60°

and 69° for GSI values of 20 and 80, respectively.) Thus, the friction angle of the Voronoi block model significantly under-predicts the friction angle of the lithophysal rock mass. Under-prediction of the friction angle bounds and over-predicts rockfall and instability.

1.2.3 Irreversible Volume Change Due to Yielding of the Rock Mass

Typically rocks exhibit irreversible volumetric strain (i.e., dilation) as a result of plastic shear deformation. The dilation is a consequence of: 1) bulking of the loose material created within the damaged zone as particles roll relative to each other, 2) mismatch of rough joint surfaces as they move relative to each other (i.e., dilation of joints), or 3) opening of tensile fractures (Kaiser et al. 2000, Section 4.1.3). The dilation of confined rock can have an effect on its further yielding, because the dilation will cause an increase in the mean stress (due to increase in volume of the confined rock), effectively strengthening the rock by increasing its confinement.

However, the dilation of the material near the free surface, such as the drift wall, will not affect the rock strength, its yielding or the extent of rockfall. The empirical (e.g., Kaiser et al. 2000, Section 3.2.2, Equation 3.3) expressions for depth of breakout or analytical stability criteria (Jaeger and Cook 1979, Section 18.2, Equation 8) are independent of rock dilation. Instead, the dilation of the failed rock will result in an increase in wall displacements or an increase in load on the ground support, if present (e.g., Kaiser et al. 2000, Section 4.1.3; Ribacchi 2000, Section 5.3).

The effect of dilation (expressed through the dilation angle) on the stability of the emplacement drifts due to thermally induced stresses and time-dependent strength degradation was investigated using the continuum method and the Mohr-Coulomb constitutive relation. The results of the simulations for a Category 1 lithophysal rock mass for dilation angles of 0° (non-associated flow rule) and 40° (associated flow rule where the dilation angle equals the friction angle), which represent the extreme conditions for rock typically analyzed using continuum models, are shown in Figure 7-43 of *Drift Degradation Analysis* (BSC 2004). (The results of simulations for other rock mass categories show qualitatively similar results in terms of extent of yielding and drift stability. With increase in the rock mass quality (i.e., the rock mass category), the extent of localized failure in the drift walls decreases while it increases in the drift crown.) In both cases, the analysis predicts a stable drift configuration. The depth of inelastic deformation is practically identical in each case.

Thus, both empirical guidelines and numerical models indicate that rock dilation does not significantly affect drift stability. Although rock dilation has a second order effect on tunnel stability, the following discussion demonstrates that the Voronoi block model represents well the dilation of brittle rock during failure (yielding) under unconfined conditions, which are poorly represented in the continuum-based models typically used in engineering practice.

The main objective of the Voronoi model was prediction of drift stability; it was not intended to assess drift wall deformation or load on the ground support. Rock mass dilation has only a secondary effect on drift stability, so model dilation was not directly calibrated. However, under uniaxial stress conditions, the Voronoi block model exhibits a volumetric response that is typical of what is observed during failure of the brittle rocks (consistent with the brittle response exhibited for the unconfined test shown in Figure 7-20 of *Drift Degradation Analysis* (BSC 2004). Under unconfined conditions, the Voronoi block model dilates significantly after the failure (Figure 7-22 of *Drift Degradation Analysis* (BSC 2004) as a result of opening of the axial cracks. The same shape of volumetric strain curve and large increase in volumetric strain when the peak strength is reached, as obtained for Luc du Bonnet granite, are shown in Figure 1-3 (Martin 1997) (The Underground Research Laboratory of the Canadian nuclear waste program in southeastern Manitoba, Canada is located within the Lac du Bonnet granite batholith.)

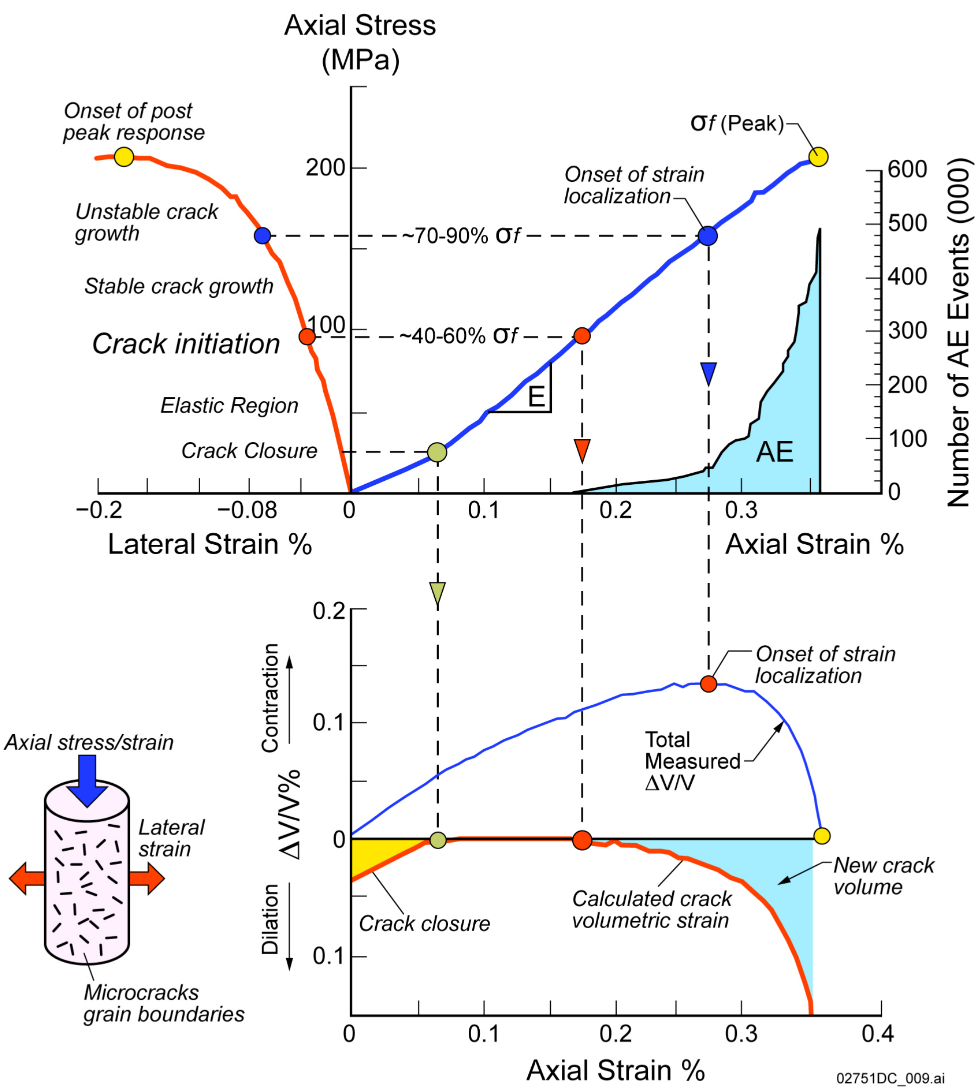

Source: Martin 1997, Figure 3.

NOTE: $\Delta V / V$ is the volumetric strain.

Figure 1-3. Three Parameters Determined from Laboratory Compression Test: Crack Initiation (σ_{ci}), Onset of Strain Localization (σ_{cd}) and the Peak Stress (σ_f)

The mechanism of lithophysal rock dilation when loaded in uniaxial compression (i.e., comparable to the loading condition for the lithophysal rock mass in the drift walls) as observed in the laboratory test and the Voronoi block simulation is illustrated in Figure 1-4. The plot of the model results includes the displacement vector field, which shows significant lateral displacement (i.e., dilation) due to opening of axial cracks (indicated in red in the figure). This volume increase, typical for failure of axially loaded rocks, is never expressed in terms of dilation angle, because the dilation angle of uniaxially loaded rock would considerably exceed the friction angle. In the classical theory of plasticity (e.g., Jaeger et al. 2007, Section 9.7), it is assumed that the dilation angle ranges between zero (no dilation) and the value of the friction angle (associated plasticity). Thus, the standard continuum models do not correctly predict volumetric deformation associated with failure of brittle rocks under unconfined conditions. Furthermore, Diederichs (2003) states:

> This is not the mechanism assumed in conventional plasticity when dilation (angle) is considered. This phenomenon presents a problem when applying conventional concepts of dilation, as implemented in numerical plasticity to post peak behaviour of spalled ground. In fact, the process of spall damage itself is incompatible with the mechanics underpinning most commonly used constitutive models for continuum geomaterials.

Although Diederichs (2003) uses the term “spalling” of rock, the discussion is applicable to general failure of brittle rocks under uniaxial conditions. The lithophysal rock mass in the drift wall will not spall by fracturing of the intact rock (as discussed in more detail in the response to RAI 3.2.2.1.2.1-001). However, unlike in typical continuum models, the volumetric response observed in the Voronoi block model is qualitatively the same as the mechanism of extension and opening of pre-existing joints during failure of the lithophysal rock mass. Because the Voronoi block model overestimates the brittleness of the lithophysal rock mass under uniaxial conditions, it also overestimates its dilation.

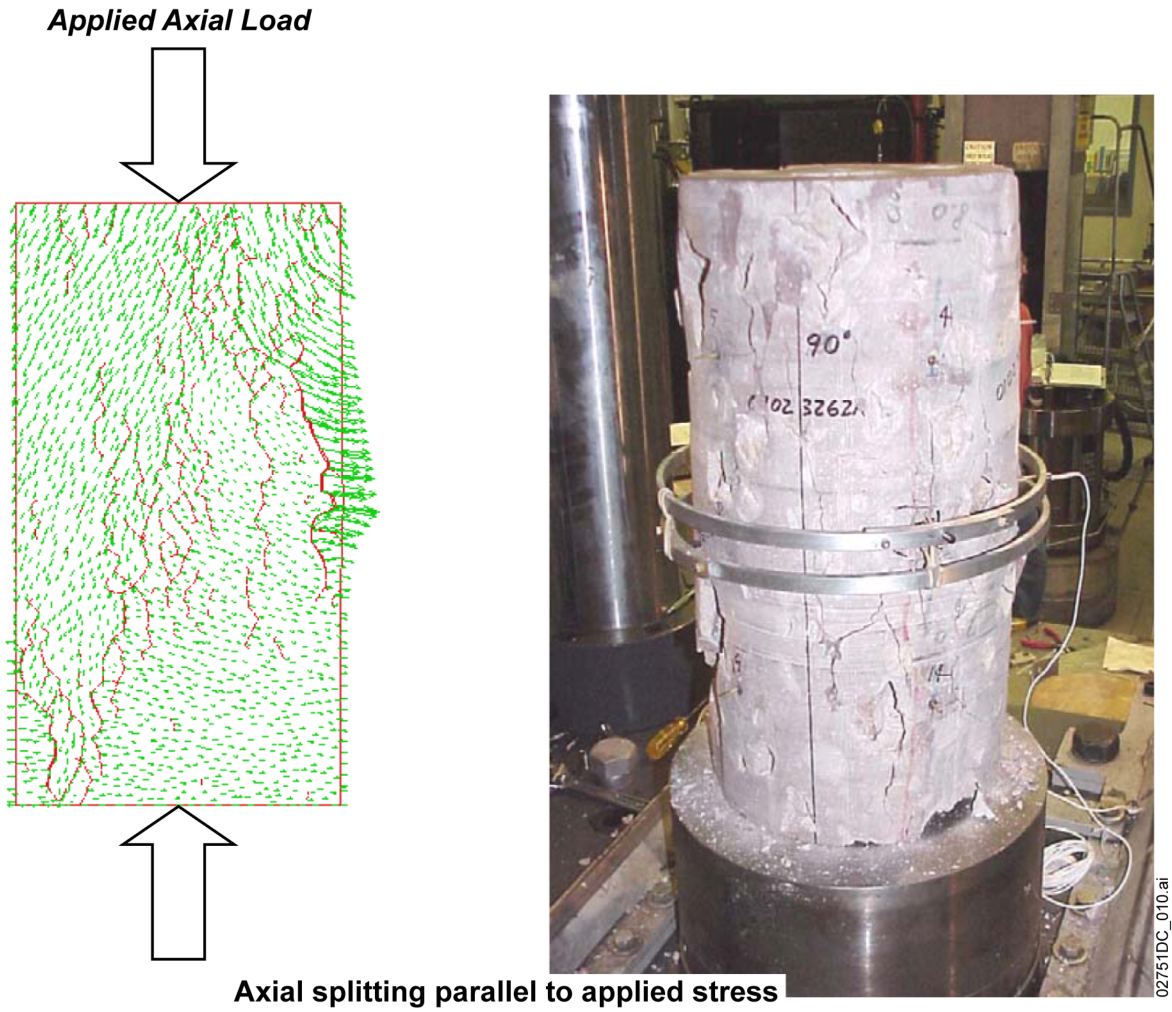

Source: BSC 2004, Figure 7-23.

NOTE: The model predicts axial splitting when no confinement is applied, as seen by the red tensile block boundary breakages (fractures) formed and by the velocity vectors that show sidewall spalling. Core photo shows a similar axial splitting phenomenon.

Figure 1-4. UDEC Discontinuum Model of Failure of Lithophysal Tuff Specimen under Uniaxial Compression (left side) and Laboratory Test (right side)

As is observed on rock samples (Ribacchi 2000, Section 5.3), the dilation of the Voronoi block model decreases with increase in confinement (BSC 2004, Figure 7-22) as overall behavior becomes more ductile, falling within the range assumed in the continuum theory of plasticity (i.e., equal to or less than the friction angle).

The Voronoi block model, unlike continuum models, correctly represents the mechanism of lithophysal rock dilation. However, dilation of the lithophysal rock mass does not affect drift stability or depth of breakout, thus the lithophysal rockfall model is insensitive to dilation.

1.2.4 Tensile Strength of the Rock Mass

The tensile strength of a rock mass is very scale-dependent. The extent and nature of discontinuities and planes of weakness of the rock mass (e.g., jointing) have a profound effect on the rock mass tensile strength. The tensile strength of the rock mass decreases as the scale increases, and more discontinuities are present. Consequently, the tensile strength that is determined on an intact, small-scale, rock sample is usually unrelated to the tensile strength of the rock mass, except in the unusual case that the large scale rock mass is unfractured. Even so, due to the impracticability of testing large-scale specimens, the tensile strength of a rock mass cannot be determined directly. As a consequence, the tensile strength of a rock mass is typically estimated based on empirical guidelines. It is often assumed to be between 1/20 and 1/10 of the UCS of the rock mass (e.g., Jaeger and Cook 1979 [DIRS 106219], Table 6.15.1).

Analyses of drift stability have shown that no macroscopic tension is ever induced anywhere near the emplacement drifts (e.g., BSC 2004, Figures 6-141 to 6-144) in the nominal scenario (i.e., in situ stress, thermally induced stresses and time-dependent strength degradation). Consequently, the tensile strength of the lithophysal rock mass has no effect on drift stability under the nominal scenario. Figure 7-21 from *Drift Degradation Analysis* (BSC 2004) shows the strength envelope for the Voronoi block model of the Category 1 lithophysal rock mass, indicates that the ratio between tensile and unconfined compressive strengths is approximately 1/14. Thus, the Voronoi block model produces a tensile strength which is within the typical range, although it has no effect on drift stability as noted above.

The discussion presented in Section 1.2 demonstrates that: 1) the model rockfall predictions are insensitive to dilation angle and tensile strength of the rock mass, and 2) the model overpredicts the rockfall as a result of its representation of the rock post-peak behavior and the friction angle.

2. COMMITMENTS TO NRC

None.

3. DESCRIPTION OF PROPOSED LA CHANGE

None.

4. REFERENCES

Bazant, Z.P. and Chen E.P. 1997. Scaling of Structural Failure. *Appl. Mech. Rev.* Vol. 50, No. 10. TIC: 260307.

BSC (Bechtel SAIC Company) 2004. *Drift Degradation Analysis.* ANL-EBS-MD-000027 REV 03. Las Vegas, Nevada: Bechtel SAIC Company. ACC: DOC.20040915.0010; DOC.20050419.0001; DOC.20051130.0002; DOC.20060731.0005; LLR.20080311.0066. (LSN# DN2002143780, DN2002140376, DN2002203028, DN2002293941, and DEN001579853)

Diederichs, M.S. 2003. The 2003 Canadian Geotechinical Colloqium: Mechanistic interpretation and practical application of damage and spalling prediction criteria for deep tunneling. *Can. Geotech. J.* Vol. 44. TIC: 260309.

Hoek, E. 2007 *[Practical] Rock Engineering, [2007 Edition]*, Toronto, Ontario, Canada: RocScience.
http://www.rocscience.com/hoek/pdf/11_Rock_mass_properties.pdf. TIC: 256345.

Jaeger, J.C. and Cook, N.G.W. 1979. *Fundamentals of Rock Mechanics*. 3rd Edition. New York, New York: Chapman and Hall. TIC: 218325.

Jaeger, J.C., Cook, N.G.W. and Zimmerman, R.W. 2007. *Fundamentals of Rock Mechanics*. 4th Edition. Blackwell Publishing.

Kaiser. P.K., Diederichs, M.S., Martin, D., Sharpe, J. and Steiner, W. 2000. Invited Keynote: *Underground Works in Hard Rock Tunnelling and Mining.* GeoEng2000, Melbourne. CDROM. 87 pgs. TIC: 254732.

Martin, C.D. 1997. Seventeenth Canadian Geotechnical Colloquium: The effect of cohesion loss and stress path on brittle rock strength. *Can. Geotech. J.*, Vol. 34. TIC: 260303.

MO0408MWDDDMIO.002. Drift Degradation Model Inputs and Outputs. Submittal date: 11/26/2008.

Price R.H. 2004. *The Mechanical Properties of Lithophysal Tuff: Laboratory Experiments*. TDR-EBS-MD-000027 REV 00. Las Vegas, Nevada: Bechtel SAIC Company. ACC: DOC.20040506.0001.

Ribacchi, R 2000. Mechanical tests on pervasively jointed rock material: Insight into rock mass behavior. *Rock Mech. Rock Engng.* 33 (4), 243-266. TIC: 260308.

SN0208L0207502.001. Mechanical Properties of Lithophysal Tuff, Batch #1 (Test Dates: July 31, 2002 through August 16, 2002). Submittal date: 08/20/2002.

RAI Volume 3, Chapter 2.2.1.2.1, Number 6

Provide a technical basis to demonstrate how the results of the drift-scale heater test are reconciled with the results of the numerical model simulation of the test. The reconciliation should address differences between rubble accumulation from the field test and the numerical model. Also, explain the implications of not modeling the field-test ground support (rock bolt and wire mesh) and three-dimensional geometry. If the drift-scale heater test is not deemed an appropriate analog for model support, then provide additional support for the model from empirical observations of heated tunnels. This information is needed to verify compliance with 10 CFR 63.114 (e), (f), (g).

1. RESPONSE

Observations of rock spalling inside the Drift Scale Heater Test (DSHT), first made in late 1999, were part of the original validation of the UDEC model for drift degradation. The DSHT was still ongoing at the time of the original validation, and the areas where loose rock accumulated were not directly accessible. The original validation was therefore based on observations of broken rock and an estimate of fracturing that were made remotely, using a rail-mounted camera (SNL 2009 [DIRS 185961], Section 3.3). The original validation is documented in Section 7.6.5.3 of *Drift Degradation Analysis* (BSC 2004).

Spalling or slabbing of the rock in the DSHT occurred during the thermal overdrive of the test, when temperatures at the rock surface were increased to almost 200°C (i.e., greater than the predicted maximum temperature around the emplacement drifts in the nominal scenario). The DSHT, which involves a 47.5-m long, 5-m diameter, heated drift, was simulated numerically in a two-dimensional UDEC model using Voronoi (polygonal) blocks to represent the host rock. The ground support (i.e., Swellex rock bolts and wire mesh), used in the crown and the walls above the springline of the heated drift, was not represented in the numerical simulation. Due to the approximate nature of the information about the extent of fracturing and volume of the loose rock (some was held up by wire mesh and some had fallen through the wire mesh to the floor), the original comparison between the numerical results and field observations was qualitative.

1.1 RECONCILIATION OF MODEL AND TEST RESULTS

When the DSHT was completed in 2006, the drift walls and crown were carefully surveyed. All damaged areas were marked by white paint, and the entire damaged surface of the drift was photographed. The process of marking and photographing the loose rock and damaged area is described in *Supplemental Rockfall Analyses for RAI 3.2.2.1.2.1-001 and RAI 3.2.2.1.2.1-006* (SNL 2009, Section 3.3). A complete set of photographs from the DSHT is provided in DTN: MO0901ROCKFALL.000 (DST submittal\file: *DST rubble zone estimation4.xls*). An example of this data, taken on the left rib, 21 m from the entry bulkhead, is shown in Figure 1-1. The wire mesh, which holds the loose rock, is built to 3-in (75-mm) squares (SNL 2009, Section 3.3). Mesh squares within the painted rubble zone were counted and used to estimate the surface area of the fractured zone. The total surface area of the fractured zone was estimated to be 37.1 m^2 (DTN: MO0901ROCKFALL.000, DST submittal\file: *DST rubble zone estimation4.xls*).

Because the endpoint station of the painted area is 34.5 m from the bulkhead (frame number 0355), the average width of the fractured zone in the plane of the drift cross-section is ($37.1\ m^2/34.5\ m$) = 1.08 m.

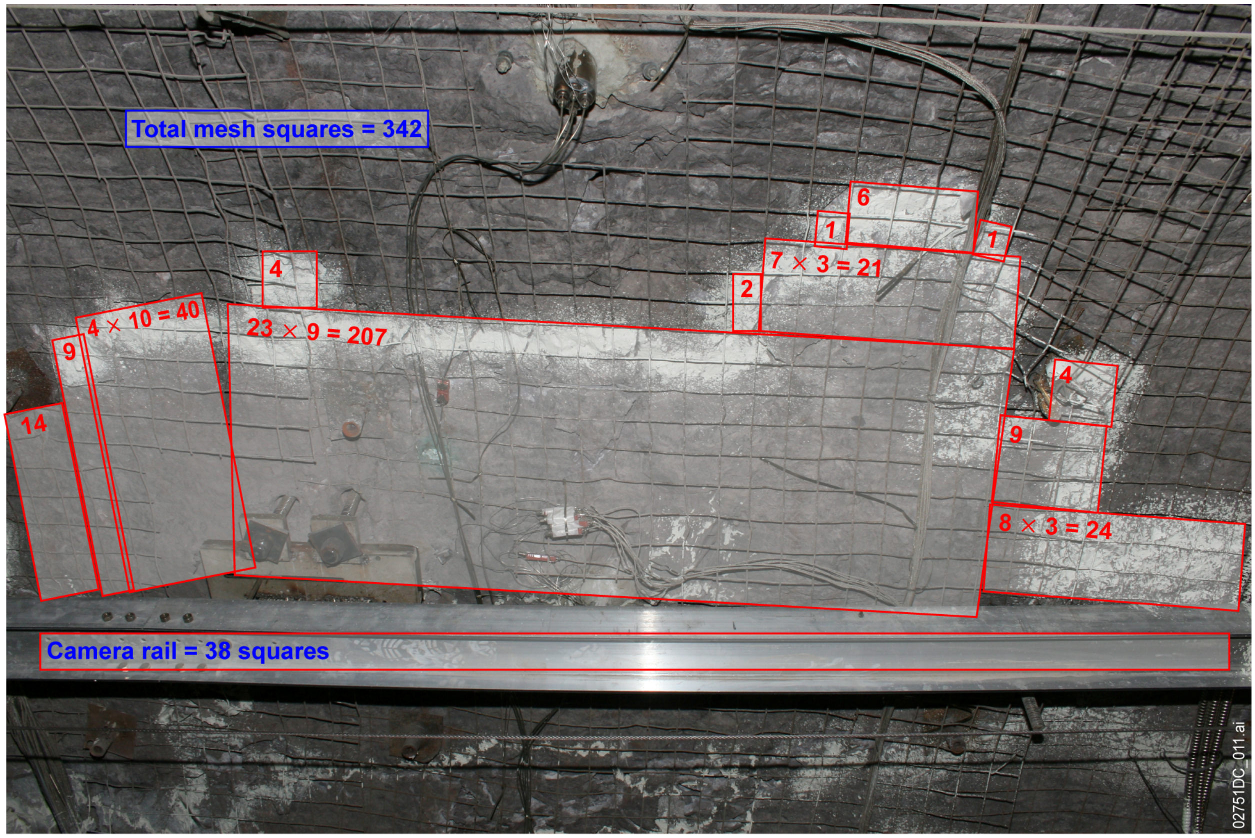

0303 left rib, 21 m from bulkhead, 180°, center

Source: DTN: MO0901ROCKFALL.000, DST submittal\file: *DST rubble zone estimation4.xls*, worksheet "left-rib photos," frame 0303.

Figure 1-1. Approximation of Loose-Rock Area (Indicated in White Paint) by Mesh Squares in Frame Number 0303 Taken on the Left Rib, 21 m from the Bulkhead

To estimate the volume of rockfall that would occur if the rubble were not held by the ground support, it is assumed that the broken rock has a "dog-ear" shape and the maximum depth of spalling is 0.3 m. The assumption is based on the following consideration (also provided in SNL 2009, Section 2.1.1).

The nonlithophysal rock where the DSHT was carried out is more massive than the lithophysal rock. Because of relatively large spacing of preexisting joints, and relatively large induced stresses compared to the intact rock strength, the thermally induced stresses caused spalling damage in the crown of the heated drift. Rock spalling occurs as a result of unstable fractures that are very close to and almost parallel with the free surface of the drift. Typically, when the equilibrium configuration is reached and unstable rock falls, spalling results in a "dog-ear" shaped breakout (e.g., Kaiser et al. 2000, Figure 2.13). The maximum depth of the "dog-ear" shaped breakout, d_f, formed due to overstress in massive and brittle rocks can be estimated from the empirical relation based on stress-to-strength ratio (Kaiser et al. 2000, Equation 3.3):

$$\frac{d_f}{a} = 1.25\frac{\sigma_{\max}}{\sigma_c} - 0.51(\pm 0.1) \quad \text{(Eq. 1)}$$

where $\sigma_{\max}$ is the maximum tangential elastic stress, σ_c is the intact rock unconfined compressive strength (determined on 54-mm diameter samples) and a is the tunnel radius. The illustration of the breakout shape, the relevant dimensions and the empirical data used to derive the linear fit are shown in Figure 1-2. This empirical relation is valid irrespective of the ground support. For example, Kaiser et. al. (2000, Section 3.2.2) state, "It is of practical importance to realize that in hard rock σ_{max} and therefore the depth of failure is insensitive to the support pressure applied at the excavation wall (for an extreme support pressure of 2 MPa the depth of failure is only reduced by 2 to 3%)." The average unconfined compressive strength, σ_c, of intact nonlithophysal rock is 189 MPa (BSC 2004, Table E-14). The maximum elastic stress is estimated from UDEC simulations of the lithophysal rock (e.g., BSC 2004 [DIRS 166107], Figure 7-36) to be approximately 90 MPa. Thus, the stress-to-strength ratio is $\sigma_{\max} / \sigma_c = 0.48$, a = 2.5 m, d_f = .09 from Equation 1, and the depth of breakout is estimated to be $d_f = 0.09 \times 2.5 = 0.225\,\text{m}$.

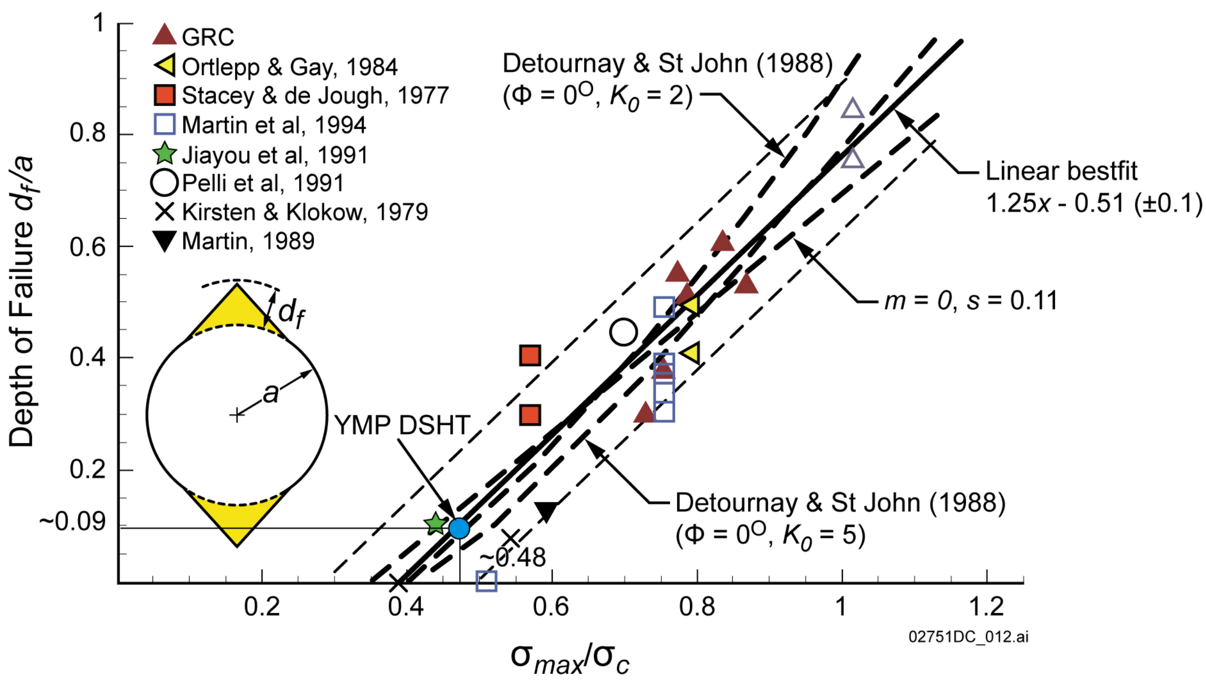

Source: Kaiser et al. 2000, Figure 3.12.

Figure 1-2 Relation of the Depth of Failure as a Function of the Maximum Boundary Stress to Uniaxial Compressive Strength Ratio for Tunnels in Hard Rock

With the assumptions of the shape and depth of broken rock (breakout), as illustrated in Figure 1-3, the estimated cross-sectional area of rockfall for the DSHT is (0.5×1.08 m $\times$ 0.3 m) = 0.16 m^2 , equivalent to a rockfall volume of 0.16 m^3 per meter of drift.

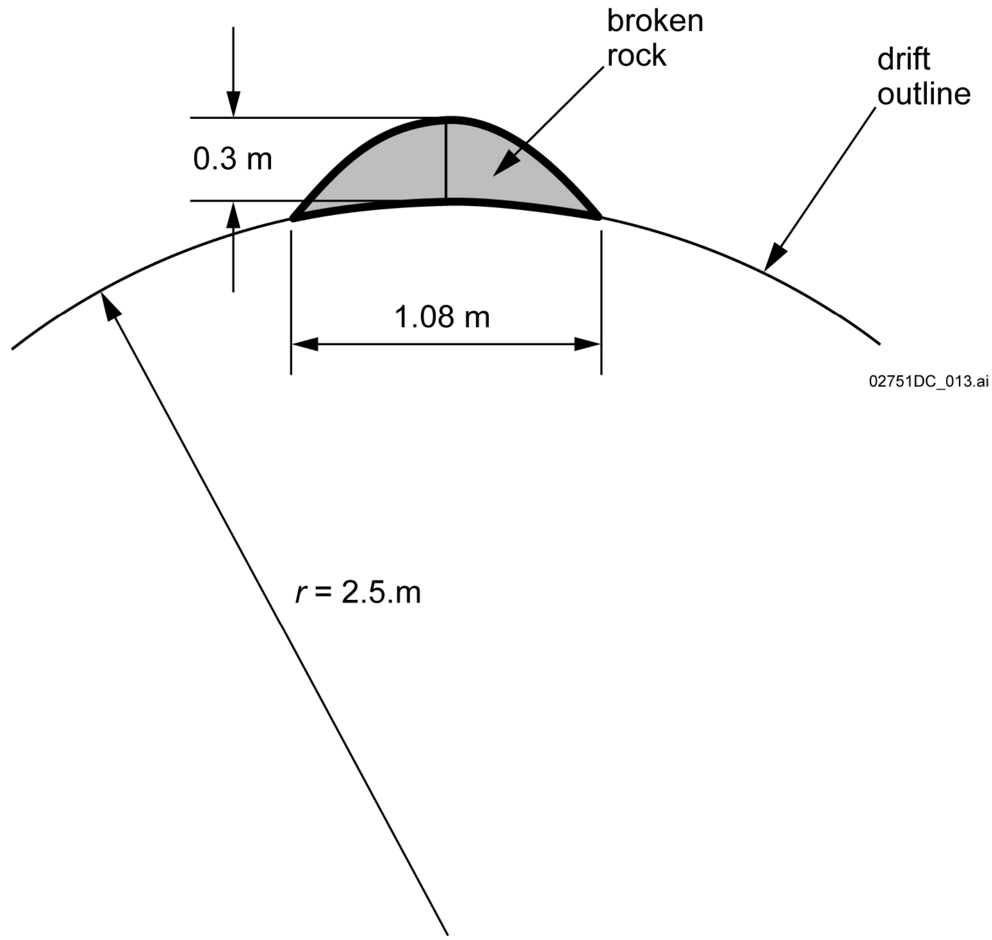

Source: For illustrative purposes only.

Figure 1-3. Geometric Configuration for Defining Maximum Depth of the Region of Spalled Rock in the DSHT

The DSHT has been re-analyzed (SNL 2009 [DIRS 185961, Section 4.2]) with two changes from the original validation analysis reported in *Drift Degradation Analysis* (BSC 2004):

The DSHT is represented as a circular tunnel of 2.5-m radius with a 1.2-m-high concrete invert, consistent with the physical configuration of the DSHT. The original analysis of the DSHT assumed a horseshoe-shaped drift cross-section, which is not consistent with the actual configuration of the DSHT.

1. The linear coefficient of thermal expansion is temperature-dependent (data for TSw2 in BSC 2004, Table E-20). The original analysis of the DSHT assumed a constant value for the linear coefficient of thermal expansion, which underestimates the thermally induced

stresses. (All other thermo-mechanical analyses described in BSC 2004 use the temperature-dependent linear coefficient of thermal expansion.)

The general numerical approach and other input parameters are unchanged from the original validation analysis.

Total volume of rock accumulated on the invert at the end of the experiment in 2006, as predicted by the sum of the area of failed rock blocks in the numerical simulation, is 0.155 m^3 per meter of drift (in the unsupported case) (DTN: MO0901ROCKFALL.000, DST submittal\unsupported\ *Case1jointing10age2006.sav*). The predicted rockfall volume is in very good agreement with the estimated rockfall volume of 0.16 m^3 per meter of drift at the completion of the DSHT. This result reconciles the results of the DSHT with the validation analyses.

1.2 IMPLICATIONS OF NOT MODELING GROUND SUPPORT AND THREE-DIMENSIONAL GEOMETRY

The ground support (Swellex rock bolts and wire mesh) was not included in the original validation analysis documented in *Drift Degradation Analysis* (BSC 2004) because both practical experience (Kaiser et al. 2000, Section 4.1.3) and modeling experience (Hoek et al. 2000, Section 10.6.1) indicate that such support has little effect on the extent of damage and fracturing of the rock mass. The purpose of Swellex rock bolts and wire mesh is simply to keep loose rock from falling on the floor, and the ground support in the heated drift served this function. The purpose of the rock bolts and wire mesh is not to prevent or reduce fracturing of the rock.

To demonstrate the effect of ground support on predicting rockfall in the DSHT, the stability of the drift during the test was simulated both with and without ground support (SNL 2009). Only the rock bolts (3-m-long Super Swellex bolts at a 1-m square pattern in the crown and the walls above the springline (SNL 2009, Section 4.2)) were included in the representation. The wire mesh was not represented because its bending and axial (in compression) stiffnesses are negligible, and it does not provide any back pressure to the rock. In fact, some pictures of the spalled zone in the drift crown (i.e., BSC 2004, Figure 7-29) show the wire mesh sagging under the weight of the loose rock. That is an indication that the flexibility of the wire mesh is such that the wire mesh allows movement of the broken rock and suspends it, but does not provide a backpressure to the rock surface.

Figure 1-4 compares the modeled drift configurations in 2002 for the supported and the unsupported drifts. Rockfall has caused a small amount of loose rock to accumulate on the invert for both drift configurations (supported and unsupported). Figure 1-4 demonstrates that the amount of rockfall and the new drift profiles resulting from the rockfall are not affected by the presence of the rock bolts.

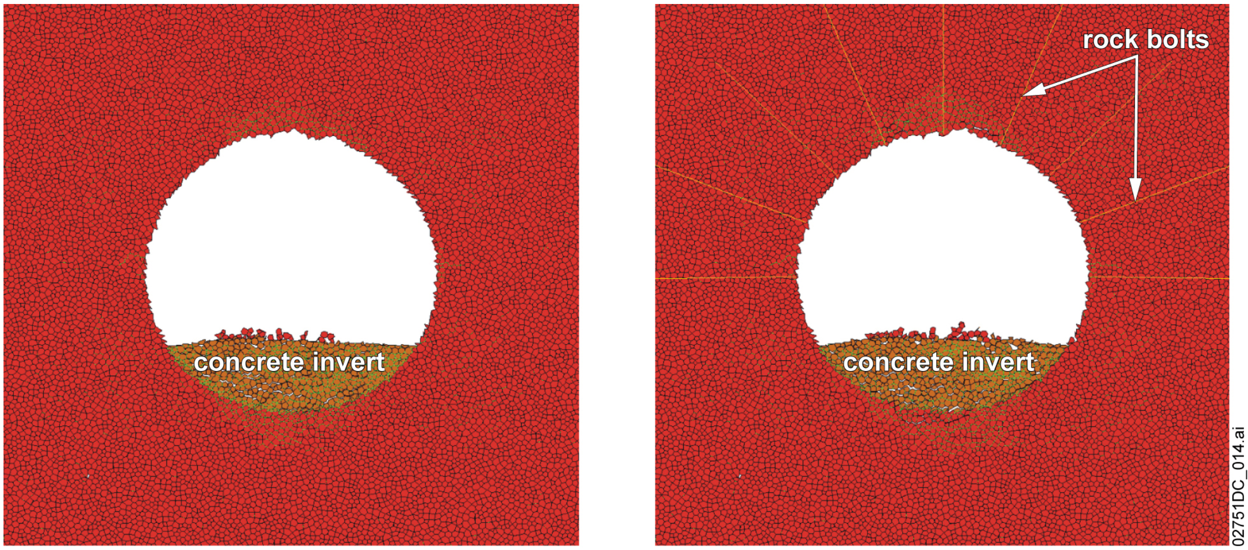

a) no support b) supported with rock bolts

Source: DTN: MO0901ROCKFALL.000, DST submittal\unsupported*plot2002.jpg*; DST submittal\supported*plot2002.jpg*.

NOTE: Figure indicates some damage and heave of the concrete floor, which has subsequently disappeared since the drift cooled down. The model overestimates the stresses and the damage in the concrete invert, which is not observed during the experiment, because of its representation of high strength in the interface between the concrete and rock. The high strength of the interface is a consequence of the exaggerated roughness in the drift outline in the model.

Figure 1-4. Comparison of the DSHT Configurations in 2002 Back Analyzed Assuming Unsupported (left) and Supported Drifts (right)

The heated drift is a 47.5-m-long circular excavation with a 5-m diameter. This geometry satisfies the condition for using a two-dimensional approximation along most of the drift length because one dimension (the axial length) is an order of magnitude greater than the other two dimensions (width and height of the tunnel cross-section). The thermal loading (i.e., due to the floor and wall heaters) is distributed uniformly along the drift length. Thus, considering the relatively homogeneous and isotropic rock mass properties (BSC 2004, Table E-15) along the heated drift, the conditions of rock deformation and yielding (during the thermal loading) are plane-strain or two-dimensional along most of the drift length.

Hoek et al. (2000, Figure 9.3) show that full tunnel convergence (as calculated from a two-dimensional, plane strain approximation) is achieved 1.5 diameters from the tunnel face. Practically, the two-dimensional approximation is adequate even at one diameter from the tunnel face. Thus, the two-dimensional approximation is adequate for 70% to 80% of the drift length.

Within 10% to 15% of the drift length from the drift face, the two-dimensional approximation underestimates deformation and damage. The drift is supported with a concrete liner between approximately the 35-m station and the drift face. Because stiffness of the concrete and the nonlithophysal rock are very similar, the three-dimensional effects exist at a short distance from the section where the concrete liner starts. (The modulus of concrete is 23.3 GPa (SNL 2009, Table 4-1); the modulus of nonlithophysal rock mass is 20.01 GPa (BSC 2004, Table E-15))

Observations from the drift (DTN: MO0901ROCKFALL.000) indicate that spalling of the rock occurred along a 34.5-m length of drift, measured from the bulkhead. The average width of the spalled rock was calculated (Section 1.1) using the actual drift length along which spalling occurred, which corresponds to the locations where plane-strain conditions are satisfied (i.e., not the entire length of the heated drift). Thus, three-dimensional effects exist along a relatively small proportion of the total length of the DSHT, and the section of the drift where three-dimensional effects exist and no spalling was observed (because the drift is supported by the concrete liner) was not considered in the validation of the numerical model.

1.3 DRIFT-SCALE HEATER TEST AS A MODEL ANALOGUE

Based on the information provided in Sections 1.1 and 1.2, the drift-scale heater test is an appropriate analogue for model validation.

2. COMMITMENTS TO NRC

None.

3. DESCRIPTION OF PROPOSED LA CHANGE

None.

4. REFERENCES

BSC (Bechtel SAIC Company) 2004. *Drift Degradation Analysis*. ANL-EBS-MD-00027 REV 03 ACN 03 ERD 1. Las Vegas, Nevada: Bechtel SAIC Company. ACC: DOC.20040915.0010; DOC.20050419.0001; DOC.20051130.0002; DOC.20060731.0005; LLR.20080311.0066. LSN numbers DN2002143780, DN2002140376, DN2002203028, DN2002293941, and DN001579853, respectively.

Hoek, E.; Kaiser, P.K.; and Bawden, W.F. 2000. *Support of Underground Excavations in Hard Rock.* Rotterdam, The Netherlands: A.A. Balkema. TIC: 252991.

Kaiser, P.K., Diederichs, M.S., Martin, D., Sharpe, J. and Steiner, W. 2000. Invited keynote: Underground Works in Hard Rock Tunneling and Mining. GeoEng2000, Melbourne. CDROM. 87 pgs. TIC: 254732.

MO0901ROCKFALL.000. Supplemental Rockfall Analyses Inputs and Outputs. Submittal date: 01/05/2009.

SNL (Sandia National Laboratories) 2009. *Supplemental Rockfall Analyses for RAI 3.2.2.1.2.1-001 and RAI 3.2.2.1.2.1-006.* PARD-MGR-DE-000231 REV 00. Las Vegas, Nevada: Sandia National Laboratories. ACC: LLR.20090122.0086. (Provided as Enclosure 8).